

I Lifetime of superheated water in a micrometric synthetic fluid inclusion

SUPERHEATING LIFETIME

MOUNA EL MEKKI¹,
CLAIRE RAMBOZ¹,
LAURENT PERDEREAU¹,
KIRILL SHMULOVICH²,
LIONEL MERCURY¹

¹*Université d'Orléans-Tours, UMR 6113 CNRS-INSU et Institut des Sciences de la Terre d'Orléans, 1A rue de la Férollerie, 45071 Orléans, France.*

²*Institute of Experimental Mineralogy, Russian Academy of Science, 142432 Chernogolovka, Russia*

I.1 Abstract.

A synthetic pure water fluid inclusion presenting a wide temperature range of metastability ($T_h - T_n \approx 50^\circ\text{C}$; temperature of homogenization $T_h = 144^\circ\text{C}$ and nucleation temperature of $T_n = 89^\circ\text{C}$) was selected to make a kinetic study of the lifetime of an isolated microvolume of superheated water. The occluded liquid was placed in the metastable field by isochoric cooling and the duration of the metastable state was measured repetitively for 7 fixed temperatures above T_n . Statistically, measured metastability lifetimes for the 7 data sets follow the exponential Reliability distribution, i.e., the probability of non nucleation within time t equals $e^{-\lambda t}$. This enabled us to calculate the half-life periods of metastability τ for each of the selected temperature, and then to predict τ at any temperature $T > T_n$ for the considered inclusion, according to the equation $\tau(\text{s}) = 22.1 \times e^{1.046 \times \Delta T}$, ($\Delta T = T - T_n$). Hence we conclude that liquid water in water-filled reservoirs with an average pore size $\approx 10^4 \mu\text{m}^3$ can remain superheated over geological timelengths (10^{13}s), when placed in the metastable field at 24°C above the average nucleation temperature, which often corresponds to high liquid tensions ($\approx -50 \text{ MPa}$).

Key Words: microthermometry, experimental kinetics, microvolumes, pure water, natural systems

I.2 Introduction

Any liquid can experience three thermodynamic states with regard to the phase diagram: stable, metastable, and unstable. When metastable with respect to its vapour, the so-called superheated liquid persists over the more stable vapour owing to the nucleation barrier related to the cost to create the liquid-vapour interface. Practically speaking, a superheated liquid undergoes any P-T conditions located between the saturation and the spinodal curves (Fig. 48). It should be noted that the term “superheating” does not refer to a particular range of temperature, and goes down to temperatures in the melting area. This superheat metastability gives to the liquid a certain “overstability feature” with respect to vapour. Indeed, geologists have long observed that liquid water displays such overstability in certain low and high temperature contexts. For instance, the soil capillary water (Pettenati *et al.*, 2008) or the water state in very arid environments like the Mars surface (Meslin *et al.*, 2006; Jouglet *et al.*, 2007) are natural examples of low T superheated liquid states whereas certain continental and submarine geysers (Ramboz and Danis, 1990) or the deep crustal rocks (Shmulovich and Graham, 2004) can also generate high T superheated solutions.

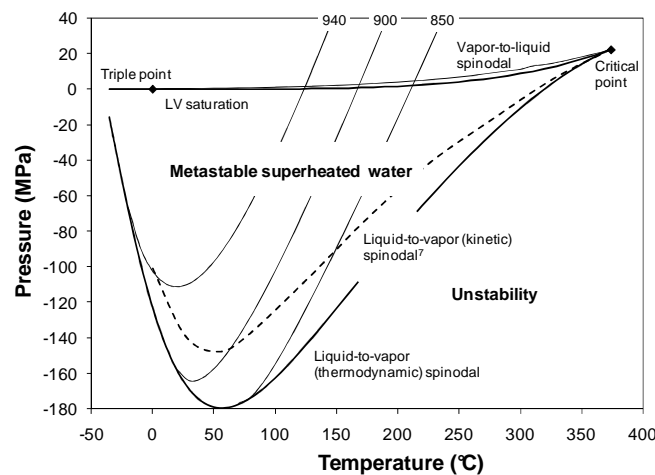


Figure 43 : Pure water phase diagram in (P,T) coordinates calculated from the IAPWS-95 equation of state (Wagner and Pruss, 2002), extrapolated at negative liquid pressures in the superheat domain. The outer lines starting from the critical point are the thermodynamic limits of metastability (spinodal). The dotted line is one of the proposed kinetic metastability limit (Kiselev and Ely, 2001) (see text). Three isochoric lines (950, 900 and 850 kg m⁻³) are also calculated by extrapolation of the IAPWS-95 equation.

The shape of the pure water spinodal has long been a matter of debate in the physics community. To date, three competing scenarios are proposed, one with the retracing shape towards positive pressure at low temperatures, the two others with a monotonous decreasing shape. The first model relates to the stability-limit conjecture (Speedy, 1982) based on experimental data on supercooled water. It can be demonstrated (Debenedetti and D'Antonio, 1986) that the retracing shape corresponds to the intersection of the spinodal curve with the Temperature of Maximal Density (TMD) line. The second proposed scenario derives from molecular simulation (Poole *et al.*, 1992) and predicts a constant positive slope, hence a spinodal monotonously extending towards negative pressures. That thermodynamically implies that this is the TMD the slope of which changes from negative to positive slope. The experimental data previously mentioned are here interpreted as related to the presence of a second critical point at low temperature and positive pressure (Poole *et al.*, 1992; Mishima and Stanley, 1998). The third proposition is the singularity-free hypothesis (Sastry *et al.*, 1996), associating a non-retracing spinodal with thermodynamic divergences. In this model, all the polyamorphic transitions of liquid water at low temperature are just relaxation phenomena and not real phase transitions, referring explicitly in that respect to the percolation model (Stanley and Teixeira, 1980). It is worth noting that most equations of state (EOS) like the van der Waals equation or the IAPWS-95 EOS result in the retracing behaviour when extrapolated in the metastable field (Fig. 48). Obviously, this is not at all an argument in support of the latter conception. However, we want to highlight that our experimental investigations are not concerned for the time being with the low temperature superheating region, so that our calculations are not influenced by this debate. The problem of the extrapolative capability of the IAPWS-95 equation remains but seems to be satisfying enough as already discussed elsewhere (Span and Wagner, 1993).

I.3 Scientific context

The chosen experimental technique to investigate the metastability liquid field is to submit to heating-cooling cycles micrometric volumes of fluid trapped in a solid fragment (Shmulovich *et al.*, 2010) This method allows measurement of the nucleation temperature (T_n) of every fluid inclusion (IF) in the host crystal, which is an evaluation of the extreme metastability that the given intracrystalline liquid can undergo before breaking instantaneously (over the

experimental time, this occurs within some tenth of seconds). By this method, the extreme tensile strength of one specific liquid (pure water, aqueous solutions...) can be directly recorded. Previous measurements provided evidences that water and in general aqueous solutions can reach very high degrees of metastability (tension reaching hundreds of MPa) (Roedder, 1967; Alvarenga *et al.*,1993). As a matter of fact, every inclusionnist (geologist dealing with fluid inclusions) is faced to the superheating ability of these micrometric fluid systems, which appears in general as a nuisance as it prevents further measurements of phase equilibria. On the other hand, a superheated liquid experiencing properties in the stretched state (negative pressure domain) displays specific thermodynamic properties. Hence distinctive solvent properties can be expected as compared to bulk water. As an example, in the Red Sea, the abnormal thermal balance of the Atlantis II Deep lower brine⁴ has been accounted for by an influx of hypercaloric superheated brines (Ramboz and Danis, 1990).

As noted above, a metastable liquid can be superheated to a very high degree before nucleating a vapour instantaneously. In kinetic terms, this means that the nucleation energetic barrier is of the same order of magnitude as the thermal energy kT of the system. This spontaneous nucleation limit is sometimes called the kinetic spinodale (Kiselev and Ely,2001) (Fig. 48). When one goes towards PT pairs greater than those of the kinetic spinodal, the nucleation barrier becomes greater than the thermal energy and the lifetime becomes longer. Generally speaking, the Classical Nucleation Theory (CNT) tells us that the nucleation rate of vapour bubble follows an Arrhenius law (Debenedetti, 1996):

$$J = J_0 \times e^{-\frac{\Delta F^*}{kT}} \quad (1)$$

where J is the number of nuclei per unit volume per unit time, J_0 is a kinetic pre-factor, E_b is the nucleation energy barrier related to the energy of interface creation.

The nucleation barrier is easy to formulate considering that the created gas-liquid interface related to bubble nucleation increases the system energy by $4\pi r^2\gamma$ (r is the radius of the spherical bubble, and γ is the liquid-vapour surface tension), while the formation of the most stable phase provides bulk energy ($4/3\pi r^3\Delta P$, with $\Delta P = P_{LIQUID} - P_{VAPOUR}$). According to the CNT, the competition between these two opposite effects results in an energy barrier E_b (Debenedetti, 1996):

$$\Delta F^* = \frac{16\pi\gamma^3}{3\Delta P^2} \quad (2)$$

E_b is reached when the spherical bubble reaches a critical radius $r_c = \frac{2\gamma}{\Delta P}$.

According to (1), P, the probability of nucleation in a volume V and during a given timelength t is:

$$P = 1 - e^{-JVt} \quad (3)$$

Nucleation is assumed to occur when $P = 0.5$. Then, the half-life period τ (median value of duration) required to get at least one vapour nucleus is :

$$\tau = \frac{\text{Ln}(2)}{JV} \quad (4)$$

Thus, the time necessary to create a bubble nucleus is inversely proportional to the fluid volume. In other words, if one second is sufficient to create one nucleus in a volume of 1 litre, more than 11 days are required in a volume of 1 mm^3 . Statistically, almost 32 000 years are necessary to do so in a volume of $1000 \text{ }\mu\text{m}^3$, a typical size for interstitial pores in most natural porous media. This calculation is made at constant J, namely for a given value of E_b , i.e., at constant metastable “intensity” and heterogeneous nucleation conditions (due to impurities in the liquid or to solid surface singularities). Thus, at constant physico-chemical conditions, nucleation is an event that becomes rarer as the fluid container is smaller. This is why soil scientists recently proposed that capillarity can occur without meeting the Young-Laplace condition, and so capillary water and its special superheating properties can occur in the whole range of microporosity, thus affecting rather large amounts of soil water¹.

The consequences of superheating in natural systems are twice. In contexts of high thermal anomalies (geyser, phreato-magma), the changes in the fluid properties at the nucleation event (relaxation of the superheating features) may have drastic physical consequences: rapid volume changes at the phase transition, potentially accompanied by deep changes in fluid speciation. This implies explosivity and massive solid precipitation (or massive dissolution depending on the role of superheating on the rock-solution equilibria). In dry environments, superheating is a long-lived process controlled by the aridity of the atmosphere (soil capillarity). The rock-water-gas interactions thus involve a superheated liquid component which modifies the chemical features of the resident solutions (Pettenati *et al.*, 2008). Whatever the superheating context, once a natural system becomes metastable, its effective influence will depend on the duration of the metastable state, as both chemical and heat exchanges also require long time to be fully achieved.

I.4 Samples.

The fluid inclusion chosen in this study was selected among the ones previously synthesized to investigate the extreme tensile strength of liquids, depending on composition and density¹⁴. Our experimental procedure is similar to that adopted in a previous paper (Takahashi *et al.*, 2002). The selected inclusion was placed in a superheated state at a given $T > T_n$ by isochoric cooling, then we waited for the bubble to nucleate. Different intensities of liquid stretching were tested, as the same experiment was performed at 7 different temperatures above T_n . Note that T_n fixes the maximum stretching intensity sustainable by the selected inclusion. According to the CNT and as confirmed by previous experiments (Takahashi *et al.*, 2002), the distribution of metastability lifetimes is expected to display an exponential decrease.

The chosen fluid inclusion (N31-7) is located in a 450 μm -thick quartz fragment and is located 77 μm -deep below the crystal surface. It is quite big, 64- μm long and 20 μm -wide (estimated volume $\approx 8600 \mu\text{m}^3$) with a long appendix indicating a process of necking down (Fig. 49).

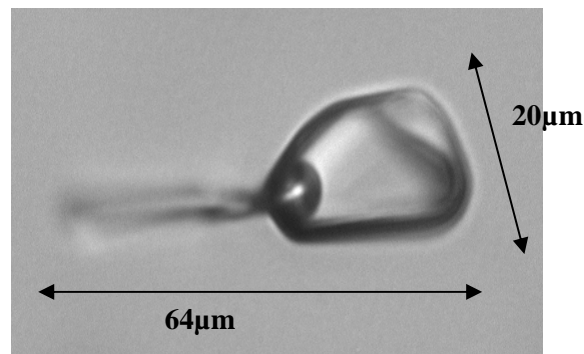


Figure 44 : Microphotograph of the studied pure water synthetic fluid inclusion (x50).

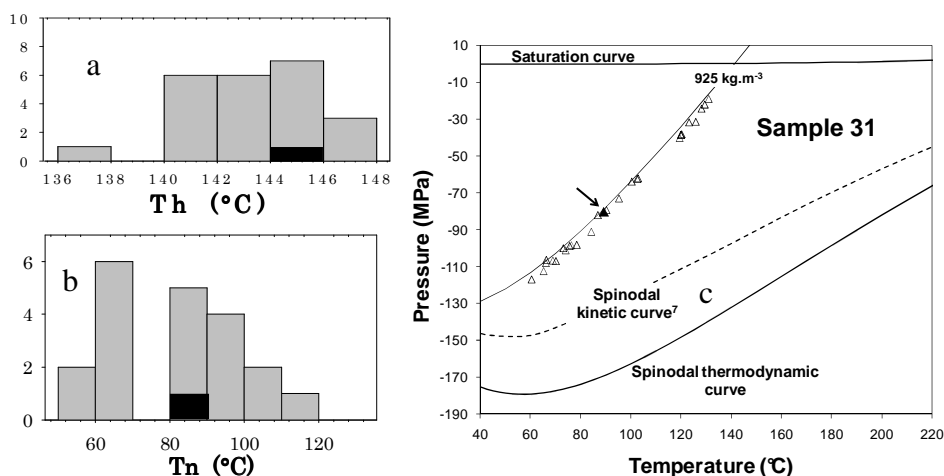


Figure 45 : Properties of sample N31 pure water fluid inclusions. Figs 50a and 3b: Distribution of T_h and T_n measurements. Fig. 50c: PT conditions of nucleation of sample N31 inclusions (triangles), with the average corresponding isochore ($d = 925 \text{ kg m}^{-3}$) extrapolated in the metastable field. The PT pure water phase diagram, the isochore and data points are calculated after IAPWS-95 EOS (Wagner and Pruss, 2002). The dark areas and arrow indicate the position of the studied $n^{\circ}31-7$ inclusion (see text).

This inclusion belongs to quartz sample N31, which contains pure water synthetic inclusions with an average density of 925 kg m^{-3} . Note that as quartz is incompressible below 300°C , the PT path followed by the inclusion fluid at changing T is isochoric (constant volume, constant density). The average isochoric PT path of sample 31 inclusions is shown in Figure 50, together with their representative points at T_n . The internal pressure at T_n is calculated from the density- T_n measurements on extrapolating the IAPWS-95 “official” pure water EOS (Wagner and Pruss, 2002). This equation also allows to derive the thermodynamic fluid properties of pure water at given P-T pairs (see reference Shmulovich *et al.*, 2009 for more details).

I.5 Experimental procedure

Sample 31 quartz fragment was placed on a Linkam heating-cooling stage mounted on a Olympus BHS microscope. Its temperature was allowed to vary (Fig. 51). Phase changes in the inclusion were observed with a x50 LWD objective and were recorded using a Marlin black and white camera (CMOS 2/3" sensor, ≈ 15 pictures/s).

I.5.1 Microthermometry

The key characteristics of the studied N31-FI7 fluid inclusion are the homogenization and the nucleation temperatures (T_h and T_n , respectively). T_h is the disappearance temperature of the last drop of vapour in the cavity (at T_h , the saturation conditions are met). T_n ($T_n < T_h$) is the measured temperature when the trapped metastable liquid becomes diphasic (it marks the end of the stretched metastable state). T_h and T_n were measured, in that order, in the course of strictly temperature-controlled heating and cooling cycles (T_h : path 1 to 4; T_n : path 4 to 6, Fig. 51).

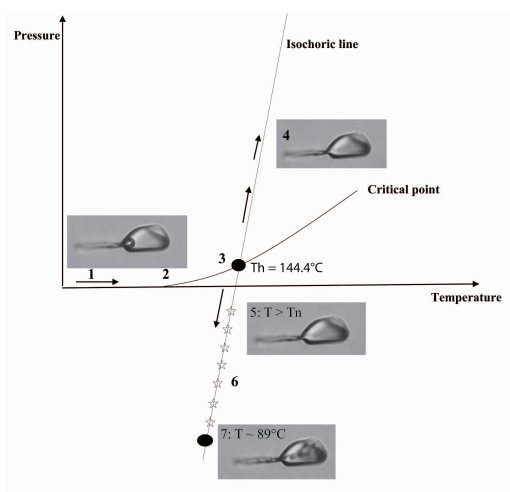


Figure 46 : PT pathways followed by a fluid inclusion heated from ambient conditions (path 1 to 4) then further cooled. Photomicrographs show the successive occluded fluid states observed. The bold curve is the saturation curve and the stars qualitatively represent the seven temperature steps chosen for the kinetic study.

Tableau 8 : Rate-controlled sequences of heating and cooling chosen for T_h and T_n measurements. First, heating along the liquid-vapour curve (diphasic inclusion), then isochoric heating followed by isochoric cooling down (single-phase inclusion).

T range (°C)	Heating cycle (T_h measurement)				Cooling cycle (T_n measurement)	
	25 - 130	130- 140	140-150	150- 160	160-105	105-80
			$T_h=144.4$			$T_n=89$
Heating/cooling rate (°C/mn)	30	10	2	10	30	2

Table 8 summarizes the rates of temperature change that were adopted all along the kinetic study. A cooling rate of 2°C/min was chosen to measure T_n as it offers the best conditions to observe bubble nucleation.

I.5.2 Kinetic measurements

Consisted in placing inclusion N31-FI7 in the metastable field. The procedure was the same as for T_n measurements except that, during cooling, the inclusion was stabilized at 1°, 1.3°, 2°, 3°, 3.5°, 4° and 5°C above T_n, successively (stars Fig. 51). The inclusion was thus kept metastable at 7 fixed temperatures between 90.4° and 94.4°C. For each given temperature, the duration of metastability was measured repetitively (between 5 and 16 metastability lifetime measurements). The beginning of the temperature step was taken as the starting point of the experiment (time 0). Between each set of kinetic measurements at a fixed temperature, we checked that T_h and T_n had not changed significantly.

I.6 Results

I.6.1 Microthermometry

At the start of the study, T_h and T_n measurements of inclusion N31-FI7 were repeated 11 times, following the T procedure summarized in Table 1. Measured T_h and T_n were 144.4° and 88.8°C respectively, with a repeatability of ±0.2°C for T_h and of ± 2.3°C for T_n. Thus the measured range of metastability for inclusion N31-FI7 was 54.6° ± 3.3°C (Table. 9), corresponding to internal P conditions of – 84 ± 4 MPa.

Tableau 9 : Repetitive cycles of T_h and T_n measurements.

T(°C)	1	2	3	4	5	6	7	8	9	10	11
Th	144.4	144.4	144.4	144.2	144.2	144.2	145.1	145.1	144.4	144.4	144.4
Tn	89.8	89.8	86.5	86.5	87.0	87.5	87.5	89.8	91.2	87.2	87.2
Th-Tn	54.6	54.6	57.9	57.9	57.24	56.7	56.6	55.3	53.2	57.2	57.2

We observed more than 50 vapour nucleation events in the IF, which enabled us to identify the main stages of nucleation. The two-phase stable situation was recovered within about 1/3s (5 to 6 images with our camera). In general, nucleation started in the broadest part of the inclusion by foam, a milky cloud a little more contrasted than the liquid. Then, a burst of tiny bubbles, taking birth in the inclusion appendix, invaded the whole cavity (Microphotograph N31-FI7, Fig. 49).

I.6.2 Kinetic results

Figure 52 shows the distribution of kinetic measurements for 7 temperature steps between 90.4° and 94.4°C (duration times in logarithmic scale).

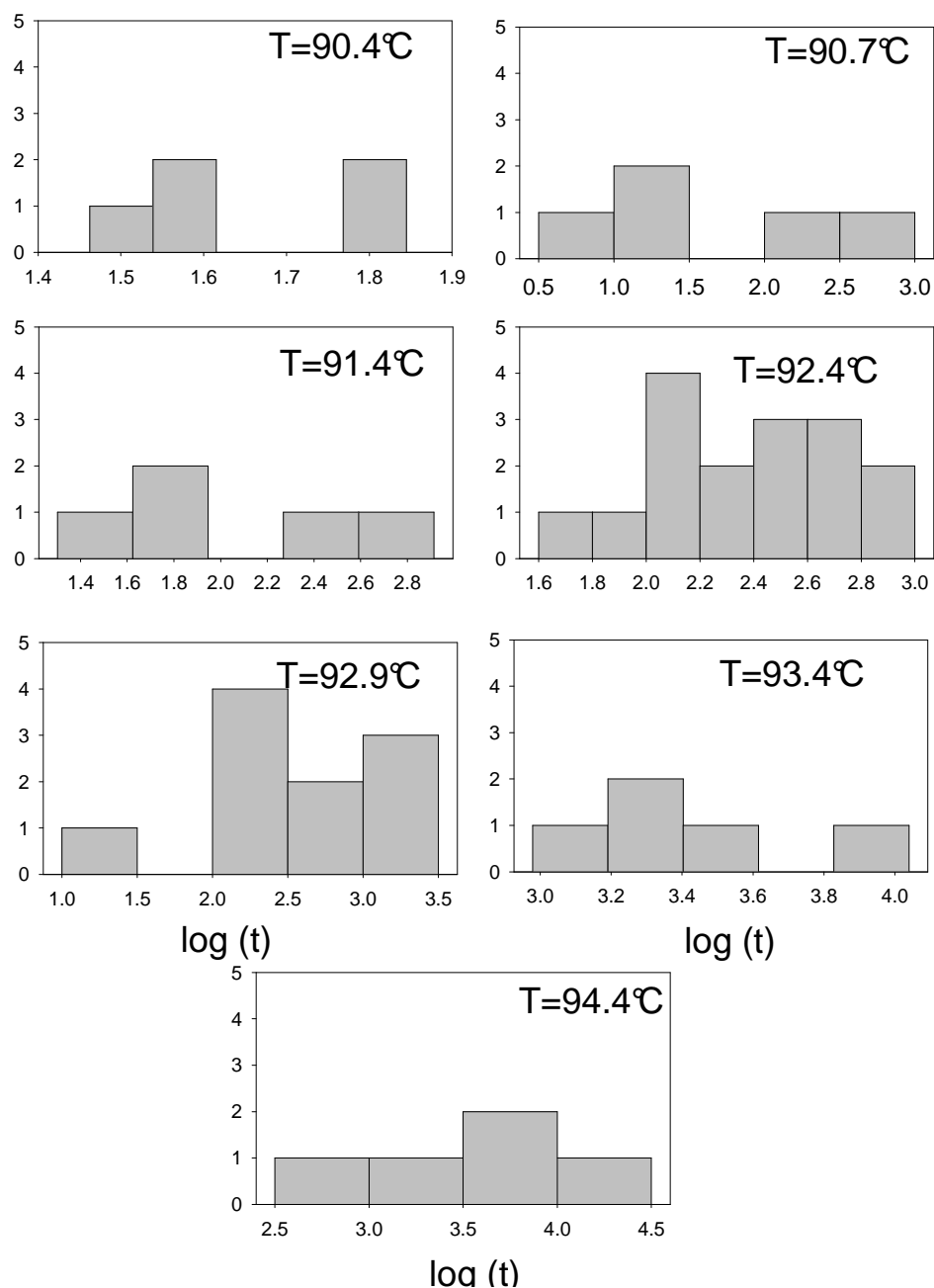


Figure 47 : Distribution of the measured metastability lifetimes (s) of inclusion N31-FI7 (logarithmic scale) for 7 temperature steps above T_n .

I.7 Interpretation of the kinetic data sets

Let T_{step} be the temperature above T_n at which inclusion N31-FI7 is stabilized in the metastable liquid state. Let t_0 be the time at which the temperature step begins (t_0 is taken as 0). Let t_i be the timelength elapsed between t_0 and the vapour nucleation event ($t > 0$). The variable t is continuous and characterized by a density probability function $f(t)$ such that:

$$\int_0^{\infty} f(t)dt = 1$$

According to the Classical Nucleation Theory, the repetitive formation of nuclei in a metastable liquid can be considered as a sequence of independent events and the distribution of metastable lifetimes shows an exponential decrease (see also Takahashi et al., 2002). This implies that the density probability function $f(t)$ of the nucleation event is:

$$f(t) = \lambda \times e^{-\lambda t} \quad (5)$$

where λ is the exponential decay constant and $1/\lambda$ the mean life of the metastable state.

The probability that the vapour bubble nucleates within timelength t is thus:

$$P(E \leq t) = \int_0^t \lambda e^{-\lambda t} dt = 1 - e^{-\lambda t} \quad (\text{Exponential Failure distribution}) \quad (6)$$

The probability of non nucleation of the vapour bubble within timelength t is

$$P(E > t) = e^{-\lambda t} \quad (\text{Exponential Reliability distribution}) \quad (7)$$

Calculation of the decay rate λ and half-life period τ at a fixed temperature step: At each temperature step, we have built the exponential reliability distribution, i.e., the probability of the non nucleation event within timelength t ($P(E > t)$). The $\text{Ln}[P(E > t)]$ were plotted versus timelength t and the data were fitted by a straight line passing by the origin (Fig. 53; correlation coefficients of the fits ranging between 0.84 and 0.99, Table 10).

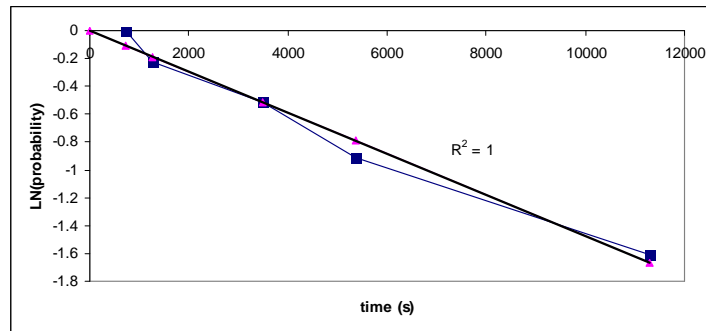


Figure 48 : Observed Fiability law at the temperature step $T = 94.4^{\circ}\text{C}$.

Hence we derived the exponential decay constants λ for the 7 T-steps considered (Table 10).

The half-life period τ at each T step was then calculated as follows:

$$\tau = \frac{\text{Ln}(2)}{\lambda} \quad (8)$$

Tableau 10 : Exponential decay constants λ calculated from the reliability distributions observed at each temperature step, and: half-life periods τ related. R is the correlation coefficient of the linear fit of the data (see text). Number between brackets = number of t measurements.

Temperature (°C)	Exponential Fiability model		
	λ	R^2	τ
90.4 (5)	0.0169	0.84	40.9
90.7 (5)	0.0046	0.94	149.5
91.4 (5)	0.0021	0.90	322.9
92.4 (16)	0.0024	0.99	286
92.9 (10)	0.00068	0.93	1025
93.4 (10)	0.00059	0.97	1166
94.4 (5)	0.000147	0.99	4702.1

On Figure 54, the calculated τ are plotted as a function of ΔT , the temperature distance to T_n (i.e. $T-T_n$). The τ values decrease exponentially as a function of ΔT , with a fitted decay constant close to 1. Due to the fact that the fitted pre-exponential factor is different from 1, we calculate a half-life period at T_n of about 22s instead of 0. On account of the heating rate adopted close to T_n (see Table 8), this indicates that the nucleation event started on average $\approx 0.7^\circ\text{C}$ before the beginning of the temperature step during cooling, our chosen time zero. Given that the measured variability on T_n is $\approx 2.3^\circ\text{C}$ (Table 9), these results corroborate our choice of placing the starting point of the kinetics experiment at around the beginning of the temperature step, rather than at T_h , as previously proposed (Takahashi *et al.*, 2002).

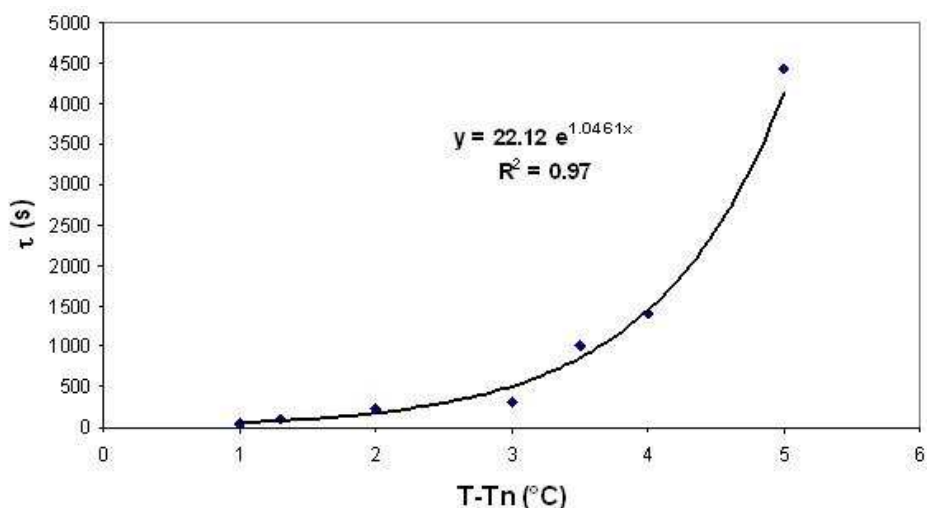


Figure 49 : Inclusion N31-FI7: Half-life period of metastability as a function of the intensity of superheating ($T-T_n$). T_n corresponds to the maximum degree of metastability sustainable by the inclusion.

I.8 Geological implications

Our data show that at a temperature of 24°C above T_n , an occluded liquid with a volume of $\approx 10^4 \mu\text{m}^3$, undergoing a tension of ≈ -50 MPa, can sustain such a high superheated state during 10^{13} seconds. A first consequence is that the half-life duration of metastability of such a system, one order of magnitude larger than one million years, is quite relevant to geological timescales. Secondly, it has been recently indicated that the changes in water properties related to superheating significantly influence the rock-water-gas equilibria as soon as the tensile strength of the liquid reaches -20 MPa (Pettenati *et al.*, 2008). Thus, our data prove that the metastability of micrometric fluid volumes is indeed a process of major geochemical importance.

As a conclusion, this paper, together with a companion one, firstly highlights that fluid inclusions are very adapted to the experimental study of superheated solutions at the μm - to mm-scale, both from the metastable intensity and kinetics points of view. In addition, we previously showed that aqueous fluids appear to superheat easily since all the 937 inclusions studied, containing pure water and various aqueous solutions, displayed superheating, some to very high degrees up to -100 MPa. The major point of this paper is to give the first quantitative proof that microvolumes of highly superheated water can sustain this stretched state for a very long time, infinite at the human scale. The fact that superheating modifies both the thermodynamic and solvent properties of water has already been assessed (Mercury *et al.*,

2003, 2004; Lassin *et al.*, 2005). It is here illustrated that such changes can persist over geologically-relevant timelengths, large enough for superheated fluids to become a possible controlling parameter of the evolution of natural systems.

Acknowledgements

This work has received financial support from the French Agency for Research (Agence Nationale de la Recherche), grant SURCHAUF-JC05-48942 (grant responsible: L. Mercury) and from Russian Fund of Basic Investigations, grant 06-05-64460 (grant responsible: K. Shmulovich). Finally, Jean-François Lenain is greatly acknowledged for his advices and for controlling the statistical treatment of the data.

II Kinetic law of stretched water and aqueous solutions in micrometric synthetic fluid inclusions: PART I - NUCLEATION RATES

Mouna El MEKKI¹, Claire RAMBOZ¹, Jean-François LENAIN², Kiril SHMULOVICH³

¹Institut des Sciences de la Terre d'Orléans, UMR 6113 CNRS/Universités d'Orléans et Tours, 1A rue de la Férollerie, 45071 Orléans Cedex, France.

²Université de Limoges, Groupe de Recherches Eau Sol Environnement (GRESE), 123 avenue Albert Thomas 87060 Limoges, France.

³Institute of Experimental Mineralogy, Russian Academy of Science, 142432 Chernogolovka, Russia.

* Corresponding author: Mouna.Elmekki@cnrs-orleans.fr

Keywords:

Metastability, microthermometry, lifetime, kinetic law, microvolumes, pure water, aqueous solution, natural systems

II.1 Introduction

Metastability is the persistence of a phase (solid, liquid or gas) in the stability field of another phase. Liquid, solid or gas metastability is possible because the attainment of equilibrium between any two of these phases requires the creation of an interface, which has an energy cost. Metastability is therefore a process controlled by a barrier of energy (Debenedetti, 1996; Balibar and Caupin, 2002). A specific feature of metastable phases compared to stable ones is that their duration of life is limited. Metastable phases return to equilibrium by relaxation. A metastable liquid persisting in the stability field of vapour, or a metastable vapour persisting in the stability field of liquid are called superheated. A stretched liquid is a particular kind of superheated liquid, which is at a pressure below its corresponding vapour pressure at a given temperature. The spontaneous formation of cavities in stretched liquids is called cavitation. Both theoretical arguments and experimental evidences show that superheated liquids can exist under absolute negative pressures (e.g., Briggs, 1950; Apfel, 1972; Blander and Katz, 1973; Green *et al.*, 1990; Alvarenga *et al.*, 1993; Imre *et al.* 1998; Schmulovich *et al.*, 2009). Metastable liquids, like solids - condensed phases in general - can undergo pressures (Imre *et al.*, 1998). The reason why liquids can be superheated and, unlike gases, can be stretched or only with flow is that they were characterized by cohesive forces. Energetic and structural considerations show that intermolecular attractive forces become predominant over repulsive ones in liquids under tension (Imre *et al.*, 1998).

The existence of metastable liquids was first reported by Huygens in (1662), even before the concept of barometric pressure was discovered. After being forgotten for \approx two centuries, metastability was rediscovered in the 19th century and the tensile strength of metastable liquids was first measured (see Kells, 1983 for a summary of early observations of metastable liquids). The development of the pioneer equation of state of Van der Waals (1873) was a decisive step for interpreting fluid metastability (Kells, 1983). Being both simple and built with physically significant parameters, this equation is still the basis for explaining why liquids can be stretched and why vapours cannot, and to calculate the superheating limits of liquids (Eberhart; 1973, 1974; Blander and Katz, 1975; Imre *et al.*, 1998). In the 30's to day, the Classical Nucleation Theory (CNT) developed a thermodynamic and kinetic approach of homogeneous nucleation to compute metastability.lifetimes, valid from the molecular to macroscopic scales. Since the 1950's, both experimental and theoretical efforts to investigate

and theorize liquid metastability have been continuous, particularly prompted by the development of industry and technology. The explosivity of relaxation processes in metastable liquids can cause strong damages in a wide variety of industries like underwater equipment, beverage industry, metallurgy, cryogenic fluid industry, power cycles (Fisher, 1976; Blander and Katz, 1973; Baidakov and Skripov, 1992; Nemeč; see also the review in Debenedetti, 1996, chapter 1 and references therein). Widespread natural liquid metastability can also threaten the life of human beings either directly (e.g., the nucleation of gas bubbles in blood: Swanger and Rhines, 1972; the role of aerosols in concentrating atmospheric pollutants) or indirectly, like the highly destructive phreato-magmatic or metastable geyser explosions occurring in volcanic settings or geothermal areas (El Mekki *et al.*, 2010). Contrasting with the many negative impacts of metastable liquids on human activities, is the fact that tensile aqueous liquids control many essential aspects of the biology of living organisms. Some examples are the succion of sap under tension towards the top of trees (Tyree and Zimmermann, 2002; Pokman *et al.*, 1995), the snapping shrimp *Alpheus heterochaelis* which generates sounds by provoking the nucleation of water. More essential to the existence of life is the fact that water in cells consists of confined metastable clusters markedly distinct from bulk water and plays a significant role in the coding of information by proteins (e.g., Ball, 2006). The exploitation of negative pressure in liquids for industrial purposes is now progressively developing as technology is improving and new environmental challenges are faced. For example, after the usage of many widely used solvents has been banned by the Montreal protocole, environmental-friendly superheated water extraction has replaced the classical solvent extraction technology (e.g., Smith *et al.*, 2002).

We here report on a set of kinetic data on tensile water in four synthetic fluid inclusions. They were chosen for being contrasted in volume, shape, density, chemistry and P_{cav} (Table 11).

Tableau 11 : Fluids inclusions descriptions and micro-thermometric measurements.

sample	composition	shape	density	Th(°C)	Tn(°C)	Th -Tn(°C)	Pn (MPa)	volume (µm ³)
N31-FI6	pure water	tubular	0.925	140.3	56.8	83.5	-115	578
N31-FI26	pure water	round	0.929	136.6	64.1	72.5	-102	382
N16-FI11	1M H ₂ O-CaCl ₂	tubular	0.964	204.8	153.7	51.1	-88	3690
N50-FI1	0.2M H ₂ O-NaHCO ₃	tubular	0.800	283.7	262.2	22	-17.4	9047

The fluid inclusion methodology consists in placing microvolumes of fluids trapped in a crystal on a microthermometric stage and letting them evolve along isochoric P-T paths by monitoring temperature. The mineral inclusion method is particularly suitable for studying

tensile water as it allows very easy microscopic observation of metastable fluids over a wide range of negative pressures and over considerable periods of time (see Imre *et al.*, 1998). It also yields reproducible nucleation (or cavitation) temperatures (T_n) at controlled cooling rates (dynamic measurements: Schmulovich *et al.*, 2009; El Mekki *et al.*, 2010). Nucleation pressures (P_{cav}) in FI rely on the extrapolation of isochores into the negative pressure domain using EOS. FI yielded the most extreme tensile strengths ever reported for water, starting with the first account by Roedder (1967) of highly tensile solutions in nature around -90 MPa (see the review on cavitation pressure in supercooled and superheated water by Herbert *et al.* 2006). Recently, Schmulovich *et al.* (2009) investigated in detail the effect of solution chemistry on the tensile strengths of intracrystalline water using synthetic FI. Despite the fact FI are particularly suitable for measuring the lifetimes of tensile water, only two sets of kinetic data have been reported so far. Zheng *et al.* (1991) calculated a rate of $2.4 \cdot 10^{14} \text{ m}^{-3} \cdot \text{s}^{-1}$ in one pure water synthetic FI at $P_{cav} = -140 \text{ MPa}$. Takahashi *et al.* (2002) measured lifetimes of tensile water in two natural FI and deduced nucleation rates around $10^7 \text{ m}^{-3} \cdot \text{s}^{-1}$ which changed by more than one order of magnitude in the P_{cav} range 16 - 16.7 MPa. The present kinetic report is part of a larger study which, as a whole, concerned seven fluid inclusions. Kinetic measurements were static and consisted in placing the occluded liquid in the metastable field by isochoric cooling and in measuring the duration of metastability repetitively for 5 to 7 fixed temperatures above the nucleation. In some inclusions of the studied set, the mean lifetimes of metastability either increased or decreased with time, indicating renewal or fatigue types of behaviour, respectively. The four presently selected FI showed a stationary type of behaviour, i.e., the mean lifetimes of metastability remained constant with time. Preliminary kinetic data on tensile water in one additional pure water inclusion ($d=925 \text{ kg m}^{-3}$; $P_{cav} \approx -85 \text{ MPa}$) with stationary failure distributions were already published elsewhere (El Mekki *et al.*, 2010). In this paper, following the approach of Caupin (2005), we paid a special attention to the accuracy of nucleation statistics (see chapitre I in this volume). Indeed, accurate kinetic data are a prerequisite to our objective, which is to evaluate the pertinence of aqueous fluid metastability over geologically-relevant timelengths. This requires extrapolation of tensile water lifetimes measured in the laboratory over ≈ 9 orders of magnitude! This paper mainly discusses static failure measurements in terms of a generalized kinetic law of tensile water in FI. In a companion paper, we shall discuss in more detail the controlling parameters of metastability in individual FI and the consistency between T_n and lifetimes measurements, e.g., between dynamic and static measurements on FI-hosted tensile water

II.2 Prerequisite to metastability

II.2.1 Thermodynamics

The thermodynamic features of superheated water were calculated by extrapolating the Equation of State (EOS) of water at pressure below the saturated pressure. The problem of the extrapolative capability of the IAPWS-95 equation remains but seems to be satisfying enough as already discussed elsewhere (Span and Wagner, 1993; Shmulovich *et al.*, 2009). By this way, we can extend the phase diagram of water including the metastable fields (supersaturated vapor, superheated, stretched and supercooled liquid).

It is worth noting that most equations of state (EOS) like the van der Waals equation or the IAPWS-95 EOS result in the retracing behaviour when extrapolated in the metastable field (Figure 55).

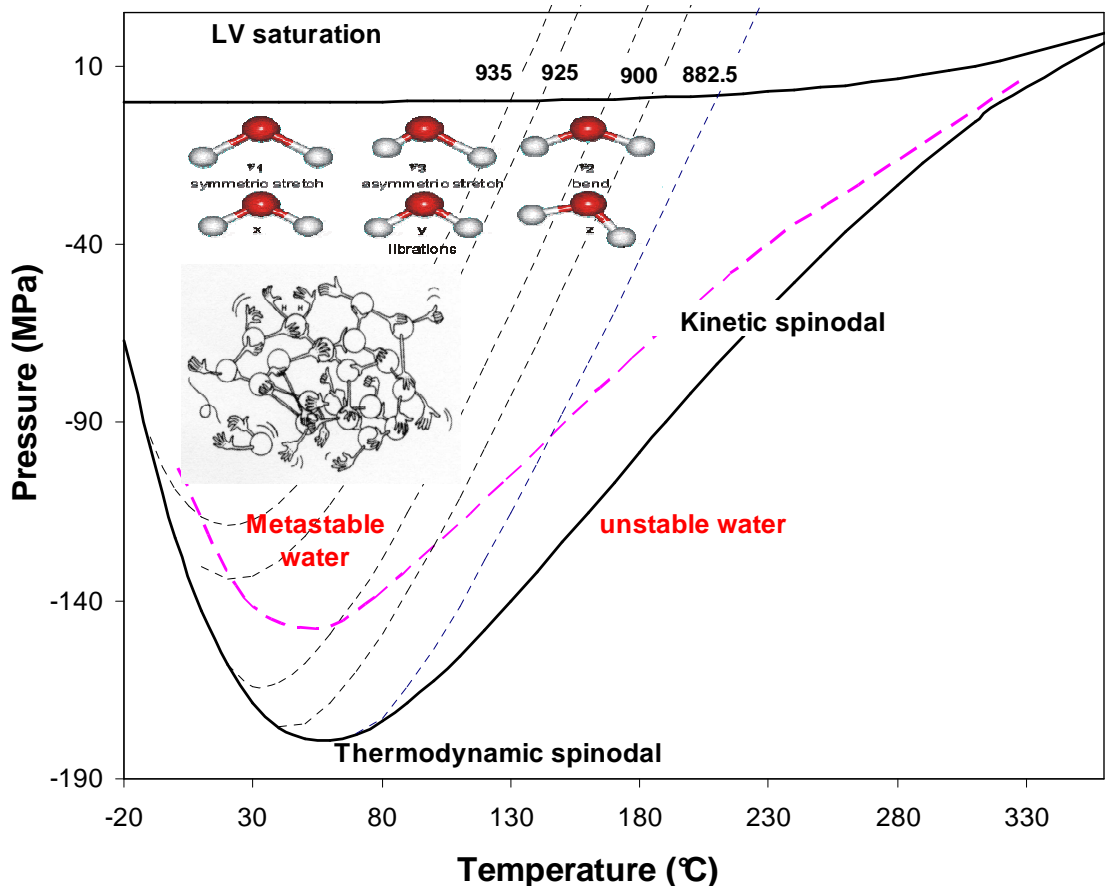


Figure 50 : Pure water phase diagram in (P,T) coordinates calculated from the IAPWS-95 equation of state (Wagner and Pruss, 2002), extrapolated at negative liquid pressures in the superheat domain. The outer lines starting from the critical point were the thermodynamic limits of metastability (spinodal). The dotted line is one maximum line nucleation. Three isochoric lines (935, 925, 900, 882.5 kg m^{-3}) were also calculated by extrapolation of the IAPWS-95 equation.

II.2.2 Kinetics

A metastable system has no thermodynamics stability. The return in the balance requires the system to reach a minimum absolute energy corresponding to the thermodynamics balance state and thus to supply an activation energy. This last one is a barrier of energy necessary for the starting up of a chemical process of nucleation. The variation of the speed of a chemical reaction according to the temperature can be described by the law of Arrhenius, which is compatible with the theory of collision and with the “sterique” effect (every atom occupies one space and the link between spaces makes a small cost of the energy) and we can write:

$$\frac{d \ln K}{dT} = \frac{E_a}{RT^2} \quad (1)$$

K, the speed coefficient, T, the temperature in Kelvin, R, the constant of perfect gas is equal to 8.314 J.mol⁻¹. K⁻¹ and E_a the energy of activation given in KJ.mol⁻¹.

We limited temperature interval and we suppose that E_a is independent from the temperature then we can integrate the law of Arrhenius:

$$K = Z\rho \cdot \exp\left(-\frac{E_a}{RT}\right) \quad (2)$$

Z is the collision frequency, the “stérique” factor; these two parameters constitute the pre-exponential factor. This law shows that the value of E_a has the dominating importance on the speed of the reactions. Then we can say that the reactions having the most low E_a are the fastest and conversely those who have the highest E_a are the slowest and it is the case in the metastable systems.

As noted above, a metastable liquid can be sustain a big traction to a very high degree before nucleating a vapour instantaneously. In kinetic terms, this means that the nucleation energetic barrier is of the same order of magnitude as the thermal energy kT of the system. This spontaneous nucleation limit is sometimes called the kinetic spinodal ([Kiselev and Ely, 2001](#)). When one goes towards PT pairs greater than those of the kinetic spinodal, the nucleation barrier becomes greater than the thermal energy and the lifetime becomes longer.

II.3 Classical nucleation theory

The classic theory of homogeneous nucleation was developed by [Volmer and Weber \(1926\)](#) and formulated by [Doring \(1937\)](#). This theory connects the nucleation rate of with the properties of surface and interface of volatile liquid in touch with the host substratum and in

the metastability degree (Blander and Katz, on 1975). The CNT includes two aspects (i) an energy aspect and ii) a statistical aspect. (i) The first point of this theory is the calculation with constant and minimal and reversible working temperature form a bubble of vapor in a homogeneous liquid phase (Abraham, on 1974; Blander and Katz, on 1975). When this minimal work is realized in temperature and volume constant the formation of vapor in the liquid is equal to the variation of free energy of Helmholtz ΔF (Hirth and al ., on 1970).

When a new vapor phase is formed in the liquid, there are two contributions in the system change. At first time, the energy decreases because the energy by unit of vapor volume is more low than the liquid, then it increases excessively the interface train between the liquid and the vapor. Thus we have a competition between the volume and the surface which have an free energy with opposite sign. This competition results a finished maximum by energy (Debenedetti, on 1996, Baidakov, on 1997) when the radius bubble reaches its critical value.

($r_c = \frac{2\gamma}{\Delta P}$ follow the Young-Laplace low), Then it decrease. The nucleation barrier (ΔF) is easy to formulate considering that the created gas-liquid interface related to the nucleation bubble increases the energy system by $2\pi r^2\gamma$ (R is the radius of the spherical bubble, and γ is the liquid-vapour surface tension), while the formation of the most stable phase provides bulk energy. ($\frac{4}{3}\pi r^3\Delta P$, with $\Delta P = P_{LIQUID} - P_{VAPOUR}$).

$$\Delta F = \frac{16\pi\gamma^3}{3\Delta P^2} \quad (3)$$

ii) The statistical aspect of the CNT concerns the nucleation rate. The nucleation rate can be seen as a flow of distribution of nucleus at critical size or as a product of a well-balanced concentration of the criticizes nucleus size n. This distribution also follows the Arrhenius law (e.g. Blander and Katz, on 1975; Cole, on 1976)

$$n = n_0 \exp\left(-\frac{\Delta F^*}{kT}\right) \quad (4)$$

n_0 is the concentration of molecules in the liquid (Hirth and al ., on 1970). This relationsheep (of n) expresses a probability of formation of nucleus is can be substituted for an equation of nucleation rate by unit of time and unit of volume (e.g. Debenedetti, on 1996):

$$J = J^0 \times \ell \exp\left(-\frac{\Delta F^*}{kT}\right) \quad (5)$$

where J is the number of nuclei per unit volume per unit time; k the Boltzmann constant , T the temperature; J^0 is a kinetic pre-factor. Le calcul de J^0 est très difficile (Maris, 2006) mais il existe deux methodes possibles pour son estimation : La première

$$J^0 = f / V_c \quad (6)$$

f a frequency factor (equal to kT/h , , h, the Planck constant), and V_c the volume of the critical nucleus (Fisher, 1948; Turnbull, 1949, Maris, 2006).

La deuxième méthode (e.g Blander and Katz, 1975 ; Cole, 1976 ; Takahashi *et al.*, 2002)

$$J^{0'} = N(2\gamma / \pi m B)^{1/2} \quad (7)$$

Where N is the density number, γ is the liquid-vapour surface tension, $B=1$ for nucleation.

According to the Reliability law, P, the probability of nucleation in a volume V and during a given lifetime t is:

$$P = 1 - e^{-Jt} \quad (8)$$

When $P = 0.5$, half of the nucleation events have occurred. The value of t for $P=0.5$ is the half-life period τ_m or median time:

$$\tau_m = \frac{\text{Ln}(2)}{JV} \quad (9)$$

Thus, the time necessary to create a bubble nucleus is inversely proportional to the fluid volume. In other words, if one second is sufficient to create one nucleus in a volume of 1 litre, more than 11 days were required in a volume of 1 mm^3 . Statistically, almost 32 000 years were necessary to do so in a volume of $1000 \text{ }\mu\text{m}^3$, a typical size for interstitial pores in most natural porous media. This calculation is made at constant J, namely for a given value of E_b , i.e., at constant metastable “intensity” and heterogeneous nucleation conditions (due to impurities in the liquid or to solid surface singularities). Thus, at constant physico-chemical conditions, nucleation is an event that becomes rarer as the fluid container is smaller. This is why soil scientists recently proposed that capillarity can occur without meeting the Young-Laplace condition, and so capillary water and its special superheating properties can occur in the whole range of microporosity, thus affecting rather large amounts of soil water (Pettenati *et al.*, 2008).

The consequences of superheating in natural systems were twice. In contexts of high thermal anomalies (geyser, phreato-magmatism), the changes in the fluid properties at the nucleation event (relaxation of the superheating features) may have drastic physical consequences: rapid volume changes at the phase transition, potentially accompanied by deep changes in fluid speciation. This implies explosivity (Thiéry and Mercury, 2009a and b) and massive solid precipitation (or massive dissolution depending on the role of superheating on the rock-solution equilibria; see also Shmulovich *et al.*, 2009). In dry environments, superheating is a long-lived process controlled by the aridity of the atmosphere (soil capillarity). The rock-

water-gas interactions thus involve a superheated liquid component which modifies the chemical features of the resident solutions (Mercury and Tardy, 2001; Mercury *et al.*, 2003, 2004; Lassin *et al.*, 2005; Pettenati *et al.*, 2008). Whatever the superheating context, once a natural system becomes metastable, its effective influence will depend on the duration of the metastable state, as both chemical and heat exchanges also require long time to be fully achieved.

II.4 Samples

Two of the FI-rich quartz samples selected for this study were synthesized following the SFI experimental technique described by Shmulovich and Graham (2004) and were previously studied by Shmulovich *et al.* (2009). Sample N50 containing H₂O - 0.2M NaHCO₃ FI is presented here for the first time. It is a quartz megacrystal which was originally synthesized for performing neutron diffraction analyses of metastable liquid water, A specific feature of this crystal is to present a wide outer growth aureole along the c-axis, with a high FI density.

Four inclusions were selected in these 3 quartz, displaying different chemistries (pure water and aqueous solutions) and variable densities, different volumes and shapes, and also variable tensile limits in the range 17 to 115 MPa (see *Table 8*).

II.4.1 Pure water Inclusions

We chose two pure water FI in quartz fragment N31 synthesized at 750 MPa, 550°C for 13 days. This fragment is approximately 450µm-thick and 2mm-wide. The selected inclusions were located ~ 80µm-deep from one crystal face. IF-6 is a 20µm-long and 4µm-wide tube (fig.2a), with a volume of 570 µm³. IF-26 is rounded and its volume is smaller (Fig.2b.; *Table 8*)

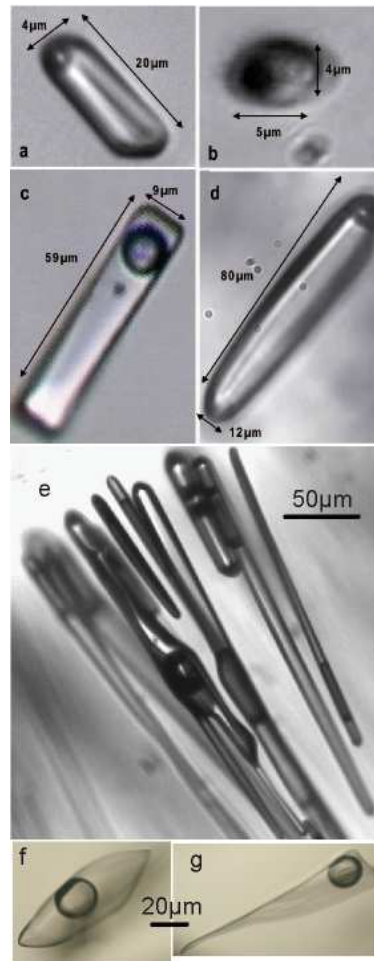


Figure 51 Microphotographs of the pure water (a and b) and aqueous solution (c) dilute $1 \text{ mol.kg}^{-1} \text{ CaCl}_2$ and $0.2 \text{ mol.kg}^{-1} \text{ NaHCO}_3$ synthetic fluids inclusions a:N31-FI 6 (x50) and b: N31-FI 26 (x80) and c:N16-FI 11 (x50) and d:N50-FI 1 (x32).

II.4.1.a 1M H₂O- CaCl₂ FI

Sample N16 was synthesized at 750 MPa, 650°C for 8 days in the presence of a H₂O-1M CaCl₂ solution. The selected N16-11 FI is tubular (Fig.2c; Table1) and located 130μm-deep into the 380 μm-thick quartz host.

II.4.2 H₂O- 0.2M NaHCO₃ FI

Sample N50 was synthesized at 750 MPa, 700°C, for 13 days in the presence of a H₂O - 0.2M NaHCO₃ solution. It was part of a originally pluricentimetric quartz monocrystal from which a ~1 cm - thick isometric fragment was first sampled. The crystal core contained scattered elongate to more isometric secondary FI with evidences of ‘necking down’ (Fig.56d, 56e). The newly-formed growth zones contained a dense network of pseudo-primary FI distributed

in 3 levels over the whole crystal thickness. The crystal growth zones displayed high liquid/solid ratio, with huge, tubular FI displaying variable lengths and widths (between 50 to 300 μm and 5 to 50 μm , respectively: *Fig. 56f*). All FI, whatever was their location in the crystal, displayed the same degree of fill ~ 80 volume % (*Fig. 56d, 56e, 56f*). The kinetic measurements on inclusion N50-FI 1 were performed on $2 \times 1 \times 1 \text{ mm}^3$ quartz prism. This FI was tubular, 12 μm -wide and 80 μm -long (bulk volume $\sim 9000 \mu\text{m}^3$), located $\sim 50 \mu\text{m}$ deep into the crystal (*Fig. 56d*).

II.5 Methods

The chosen experimental technique to investigate the liquid metastability field is based on fluid inclusions. It consists in submitting micrometric volumes of fluid trapped in a monocrystal, quartz in our case, to heating-cooling cycles (*e.g. Shmulovich et al., 2009*).

II.5.1 Microthermometry

Apparatus., The selected quartz fragments were placed on a 200 μm -thick 1.6 cm- wide rounded glass window lying on the silver block of the Linkam heating-cooling stage, with the selected FI always placed as close as possible from the silver block. Phase changes in the inclusions were observed using an Olympus BHS microscope equipped with a x50 LWD Olympus objective. Temperature was measured using a class B Pt 100 thermistance, which has an intrinsic precision of 0.15° to 1.35°C between 0° and 600°C . Temperature was sampled \sim every 400 ms by a Eurotherm 902 controller which allows analogic output. The temperature cycles of the stage (heating-cooling rates and temperature steps) were controlled using a Labview computer program (*see El Mekki et al., 2010 for more details*). Phase changes were recorded using a Marlin black and white camera (CMOS 2/3" sensor, $1280 \times 1024 \text{ pixels}^2$) at a rate of ~ 13 frames/s, limited by the data transmission rate between the controller, the computer and the stage. Temperature and time were integrated on the video image. The images were commonly compressed using the MPG4 codec before storage on the PC. Sometimes, the images were stored without compression in the vicinity of T_n in order not to degrade the image information. All T measurements were made by going through the video tape. Given that the heating or cooling rates chosen for measuring the phase changes were slow ($\sim 1^\circ\text{C}$ or $2^\circ\text{C}/\text{mn}$), temperature remained unchanged within $\pm 0.1^\circ\text{C}$ over 3 to 4 images and the change occurred within one image on the video tape.

II.5.2 Calibration

The stage was calibrated between -56.6° and 573°C using 8 reference temperatures. The standards used were natural and synthetic FI (melting point of CO_2 at -56.6°C ; melting point of ice : 0°C); ceramics (solid – solid transitions at 37° and 47°C in CsPbCl_3 and at 180°C in $\text{Pb}_3(\text{PO}_4)_2$; salt : $\beta/\gamma - \alpha$ transition at 147°C in AgI and subsequent melting at 557°C ; mineral : α / β transition in quartz at 573°C . Based on calibration, the precision on the measured temperatures is around $\pm 1^{\circ}\text{C}$ over 50° to 600°C (El Mekki *et al.*, in prep).

II.5.3 Th and Tn measurement.

The homogenization and nucleation temperatures were key characteristics of the studied FI (Th and Tn, respectively). Th is the disappearance temperature of the last drop of vapour in the cavity (at Th, the saturation conditions are met). Tn ($\text{Tn} < \text{Th}$) is the measured temperature when the trapped metastable liquid becomes diphasic (it marks the end of the stretched metastable state).

In order to carefully select the inclusions for kinetic studies based on their volume, shape, position in the crystal and metastability range, about 20 FI per sample were measured in each of the studied samples. Every measured FI was precisely located in the crystal in terms of XY and Z, the latter parameter being measured relative to a carefully identified crystal face.

The FI were heated at $30^{\circ}\text{C}/\text{mn}$ up to $\text{Th}-30^{\circ}\text{C}$. The heating rate was then decreased at 20° , 10° , 5° or $2^{\circ}\text{C}/\text{mn}$ when $\text{Th}-20^{\circ}$, $\text{Th}-10^{\circ}$, $\text{Th}-5^{\circ}$ were reached, respectively. Th was then measured at a fixed heating rate of $1^{\circ}\text{C}/\text{mn}$ (Th measurement : path 1 to 3, *Fig. 57*).

Tn measurement (paths 1 to 4 and 4 to 6, *Fig. 57*). After having reached Th, the FI is further heated by 5°C along the isochore, in order to dissolve any micro to nano bubble that could have remained attached on the FI wall. The efficiency of this procedure to limit subsequent heterogeneous nucleation was demonstrated by Ohde *et al.* (1988) and later recommended by Imre *et al.* (1998). The FI was then cooled from $\text{Th}+5^{\circ}\text{C}$ to $\sim 15^{\circ}\text{C}$ above Tn at $10^{\circ}\text{C}/\text{mn}$.

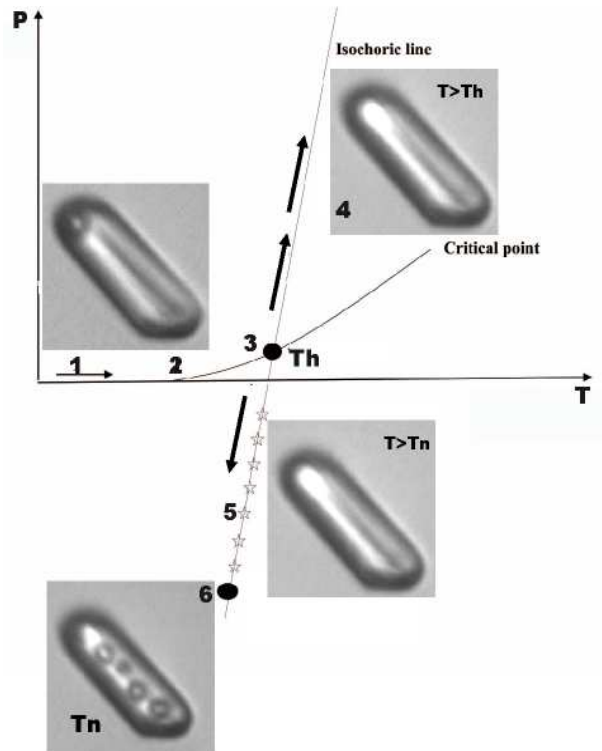


Figure 52 : PT pathways followed by a fluid inclusion heated from ambient conditions (path 1 to 4) then further cooled. Photomicrographs show the successive occluded fluid states observed. The bold curve is the saturation curve and the stars qualitatively represent the temperature steps chosen for the kinetic study.

The T_n values of inclusions N31-6, N31-26 and N16-11 were measured at a rate of $2^\circ\text{C}/\text{mn}$ and that of FI N50-1 was measured at $5^\circ\text{C}/\text{mn}$. We found that T_n measurements were unchanged and reproducible for any cooling rate less than $5^\circ\text{C}/\text{mn}$. The breaking of the metastable liquid was observed to occur within $\sim 0.5\text{s}$.

II.6 Kinetic study

Two stages were mobilized night and day for this study, for about one year and 6 months, respectively.

II.6.1 Lifetime measurements

The procedure was the same as that for T_n measurements except that, during cooling, the inclusion was stabilized at 4 to 5 different temperatures above T_n (paths 1 to 4 then 4 to 5,

Fig. 57). The inclusion was thus kept metastable at each of these temperature steps until nucleation occurred. The lifetime of metastability was noted. The starting point of each experiment was determined on the video tape as the transition point between the rate-controlled cooling path and the stabilized temperature step. Given our slow cooling rates (2° to 5°C/mn), temperature was stabilized within ~1 ms (1 or 2 images). Between each kinetic data set, Th and Tn were measured again in order to check that the FI had not been significantly changed (5 Th -Tn measurements at the minimum).

II.6.2 Optimisation of the number of lifetime measurements at each T-step

Let $\lambda=J.V$ and τ be the mean metastability lifetime ($\tau=1/\lambda$), then a confidence interval can be calculated under the exponential hypothesis with the Khi-square distribution:

$$1/\hat{\lambda}.2n/\chi_{2n;\alpha/2}^2 < 1/\lambda < 1/\hat{\lambda}.2n/\chi_{2n;1-\alpha/2}^2 \quad (9')$$

where n is the number of experiments and $\hat{\lambda}$ represents observed values and λ is the exponential decay constant. We shall further see an efficient resampling method that still gives more reliable confidence intervals. The theoretical meantime confidence interval as a function of the number of experiments n has been modelled in the case of exponential decay using equation (9') (Fig. 58). This interval is dissymmetric and becomes tighter as n increases. The experimental effort is very efficient up to n=15, efficient from 15 to 30. Larger n may have utility up to 60, depending on the kind of experiments, but about 25 observations were necessary to get precise enough intervals.

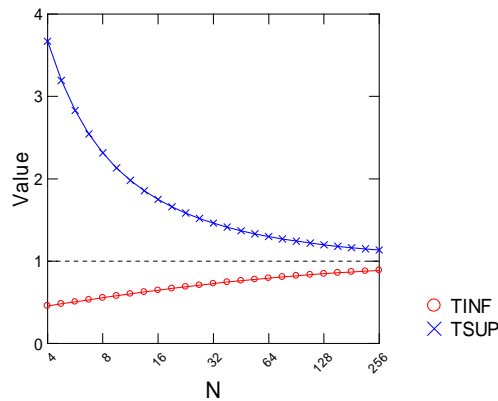


Figure 53 : 95% confidence interval of the estimated mean lifetime t in function of the number of experiments (exponential distribution). Case $t=1$ is represented; other values were deduced by a multiplicative factor t .

II.6.3 Statistical tests of nucleation rate stationarity

II.6.3.a Moving Average (MA) visual test

We used a weighted six points MA smoothing to check visually that the mean lifetime remained stable during the overall experimental time. Data were kept in experimental order and the weights are (1, 2, 4, 4, 2, 1). If the nucleation rate seemed to vary, the following tests were performed:

II.6.3.b -Non parametric Kolmogorov-Smirnov (K-S) test.

Data in experimental order were partitioned into two sub-series (T1 and T2). Then the K-S test calculated the differences between the two cumulative histograms and gave the probability p for equality (no difference) A p -value $> 5\%$ means that the difference between T1 and T2 cannot be proven, whereas a p -value $< 5\%$ means that there is a significant difference between T1 et T2 cumulative curves.

II.6.3.c Fisher test on ratios of mean lifetimes or nucleation rates

This is a more efficient test than K-S to test nucleation rate stationarity. When experimental lifetimes are exponentially distributed, the mean lifetime follows a Gamma distribution which is closely linked to Khi-2. Then the ratio of two mean lifetimes follows a Fischer F distribution. Because F is symmetric we indifferently used $T2/T1 = \lambda_{T1} / \lambda_{T2}$ or $T1/T2$. The test is bilateral and gives a probability value for equality of T1 and T2. If $p < 5\%$, then T1 and T2 differ significantly. IF $p > 5\%$, the difference between T1 and T2 cannot be confirmed and we admit that the lifetime is stationary.

II.6.3.d Test of Weibull against Exponential distribution.

Weibull is a larger model than the exponential one, where the rate increases or decreases during observation time, depending on a form parameter. Exponential is a special case when the form parameter is fixed to 1. In this case, a Likelihood Ratio Test can be driven. Given LL_e and LL_w the respective Log-Likelihoods of the two models, the difference $2*(LL_w - LL_e)$ is Khi-2 distributed with one degree of freedom. We decide that Weibull better describes the data when $2*(LL_w - LL_e)$ exceeds $\text{Khi-2}(0.95, 1) = 3.84$.

When the experimental data sample successfully went through these tests, the nucleation rate was considered as stationary.

II.6.4 Statistical methods of estimation

II.6.4.a Maximum Likelihood estimation.

It is a popular statistical method used for fitting an underlying statistical model to data, and to provide estimates for the model's parameters. In the case of the Survival law, the Likelihood function is equal to the joint probability of the observed survival times. Parameters are tuned so that this probability is maximised (in practice, the log-likelihood is maximised).

II.6.4.b Linear regression estimation of λ .

Various linearization techniques exist like probability plots. They are used to visually check the model or to give pre-estimates of the parameters. (*Fig. 59 g and h* represent Cox diagrams given by Systat)

II.6.4.c Model estimation of confidence intervals.

Under the exponential distribution of lifetimes, a theoretical interval of the mean lifetime can be estimated with the Khi-2 distribution equation (9').

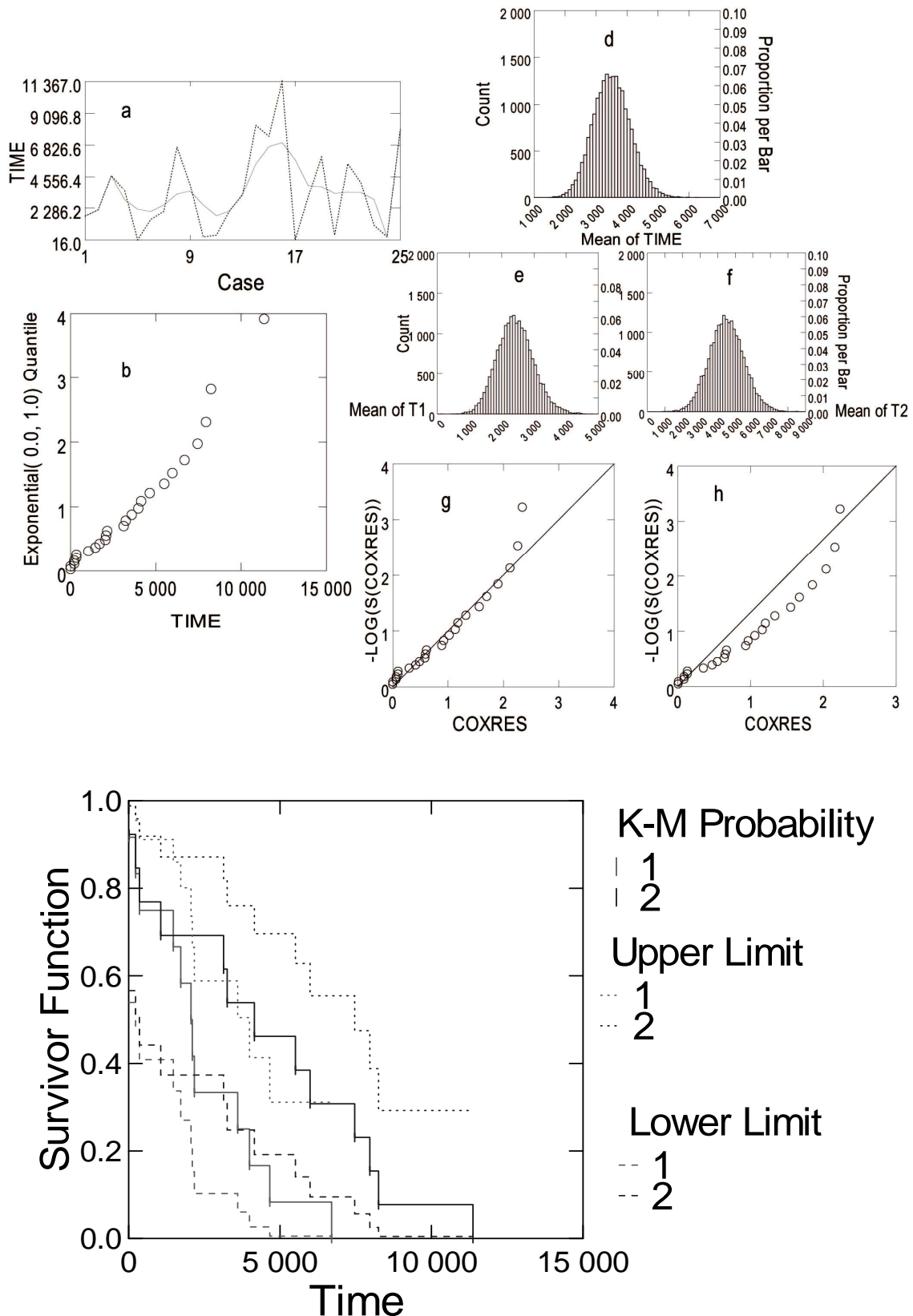


Figure 54 :.Statistical tests. Fig 6a: Le « smoothing » c'est une Moyenne Mobile pondérée faite sur six valeurs pour vérifier si la moyenne varie au cours de temps. Fig 6b: Kolmogorov-Smirnov Test Statistic. Fig 6c: Fisher test statistic. Fig 6d: Un bootsrap pour toute la série de meure. Fig 6e: Un bootsrap pour la moitié de la série. Fig 6f: Un bootsrap pour l'autre moitié des mesures de la série. Fig 5g: Ajustement de la fonction exponentielle. Fig 6g: Ajustement de la fonction weibull.

II.6.4.c.1 Bootstrap method for estimates and confidence intervals

It is a special case of Monte Carlo simulation. The first underlying principle is that the sample of measurements is the best representation we have of the distribution law. The second is that these measurements are equiprobable and therefore exchangeable between them. Bootstrapping is very useful when the probability distribution is unknown or differs more or less from the theoretical one. It is especially efficient in the case of small sample sizes. In the latter case, the bootstrap distribution is complete but the number of simulated samples increases very quickly with n (n^n). Otherwise it creates a large number of simulated samples by random sampling with replacement. Advanced Bootstrap methods add a bias correction of the estimates under the unknown distribution. In our case, let n be the number of measured lifetimes. n random sampling with replacement were performed and a mean lifetime was calculated. This procedure was repeated 10 000 times. The mean value of the Bootstrap distribution yields an optimized value of $1/\lambda$, where λ is the decay constant of the Survival law. The 95% confidence interval is defined by the values which limit 2.5% of the histogram surface area to the left and to the right.

II.7 Results

II.7.1 Microthermometry

Our Th-Tn measurements on samples N31 and N16 were consistent with the ones published by [Shmulovich *et al.* \(2009\)](#). Th and Tn were interpreted in terms of density and tensile strength, respectively, referring to the same EOS as the ones used by [Shmulovich *et al.* \(2009\)](#). The IAPWS-95 “official” pure water EOS was used ([Wagner and Pruss, 2002](#)). Density - tensile strength calculations for the H₂O-CaCl₂ synthetic FI was based on the software available at the Duan Research Group (http://www.geochem-model.org/models/h2o_cacl2/index.htm, details in [Duan and Mao \(2006\)](#)). On Figure 3, the reference spinodal curve for the latter FI is that of pure water displaced at constant shape in order to fit with the critical point of a H₂O-1M CaCl₂ solution ([Shibue, 2003](#)). Microthermometric measurements in the H₂O - 0.2M NaHCO₃ FI-1 were interpreted referring to the IAPWS-95 pure water EOS for lack of more appropriate volumetric data.

II.7.2 Samples

N31. Th's measured on 20 FI were between 136° and 148°C and the interpreted metastability range was between -38 and -115 MPa ($52^\circ < T_n < 116^\circ\text{C}$) (*Fig. 56*). Th's on these pure water synthetic inclusions define an average density of 925 kg m^{-3} . The tubular larger volume IF-6 inclusion displayed a similar tensile strength as that of the rounded smaller volume IF-26, namely -115 and -102 MPa, respectively (*Fig.2a ; Table 11*). Inclusion N31-6 enlarges the range of tensile strengths reported for pure water FI from sample N31 by [Shmulovich et al. \(2009\)](#).

Sample N16. The 20 FI measured in this sample yielded $187^\circ < T_h < 200.7^\circ\text{C}$, $145.1^\circ < T_n < 152.4^\circ\text{C}$). These results fix the average fluid density in this sample at 964 kg m^{-3} , and the range of tensile limits between -58 and -92MPa, respectively. FI-11 chosen for kinetic measurements is a large tube with sharp angles and a volume of $3700 \mu\text{m}^3$. Its tensile strength, was deduced at -80 MPa from its measured T_n at 153.7°C , intermediate between that of the pure water FI and of the $\text{H}_2\text{O} - 0.2\text{M NaHCO}_3$ FI.

Sample N50. This sample with $\text{H}_2\text{O}-0.2\text{M NaHCO}_3$ FI is studied here for the first time. It yielded higher T_h - and T_n -values than any other sample synthesized by [Shmulovich et al. \(2009\)](#). Its T_h 's and T_n 's, $(283.7^\circ < T_h < 283.9^\circ\text{C}; 262.1^\circ < T_n < 266.1^\circ\text{C})$ characterize an average fluid density of 800 kg m^{-3} and a range of metastability between -16 and -21 MPa. The selected inclusion N50-FI 1 has the lowest density and tensile strength of the 4 FI studied in this paper (*Table 11*).

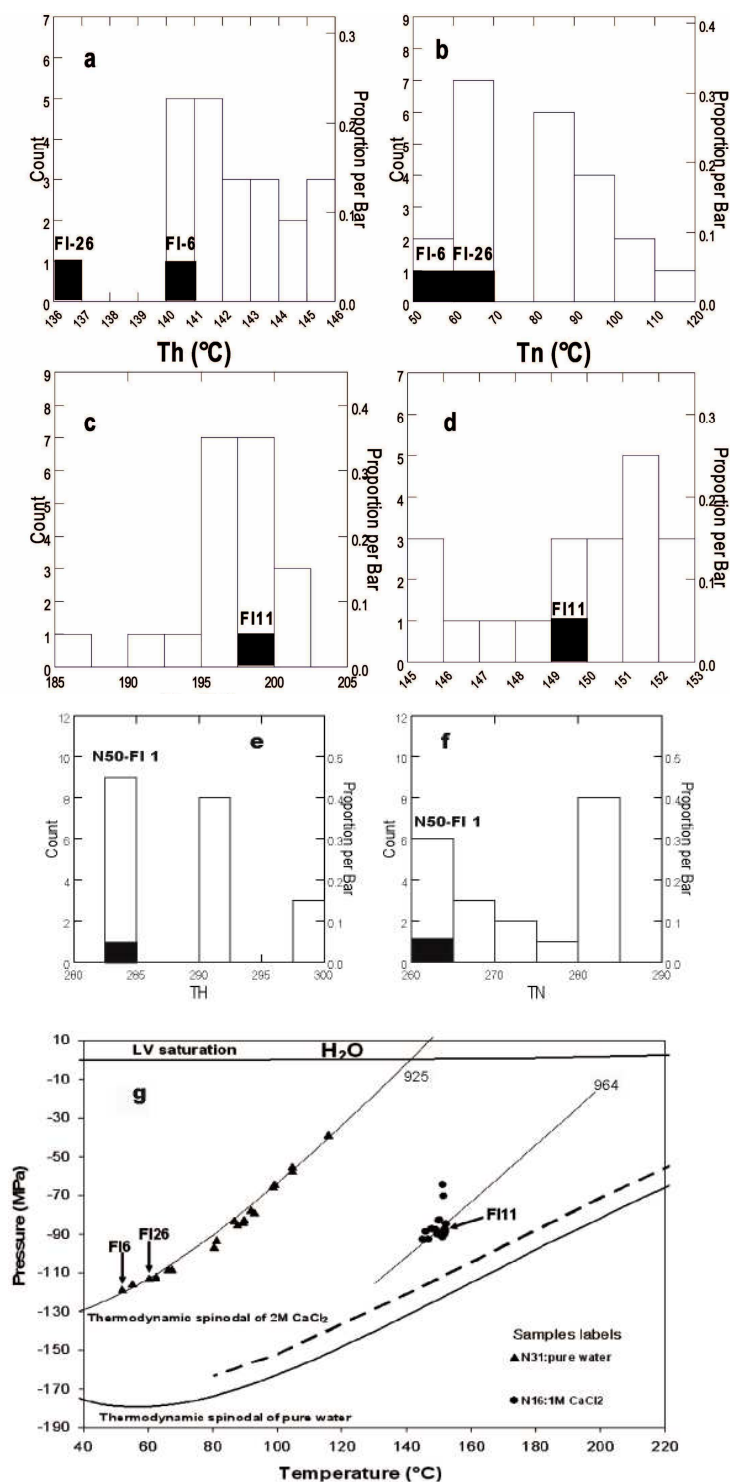


Figure 55 : Properties of samples 31 pure water and 16 dilute 1mol.kg^{-1} CaCl_2 fluid inclusions. Figs 3a and 3b: Distribution of Th and Tn measurements of sample 31 inclusions. Figs 3c and 3d: Distribution of Th and Tn measurements of sample 16 inclusions. Fig. 3e: PT conditions of nucleation of samples 31 inclusions (triangles) and N16 (circles), with the average corresponding isochores ($d = 925 \text{ kg m}^{-3}$) for pure water and the average corresponding isochores ($d = 964 \text{ kg m}^{-3}$) for CaCl_2 extrapolated in the metastable field. The PT pure water phase diagram, the isochores and data points were calculated after IAPWS-95 EOS. The thermodynamic spinodal of CaCl_2 (The dotted line) is calculated after Shibue (2003). The dark areas and arrows indicate the position of the studied N31-6 and 26 and N16-11 inclusions.

II.7.2.a Description of nucleation processes.

Nucleation is a very complex and quick process occurring within about 1/3s corresponding to about 5 or 6 images on our Marlin camera. The nucleation process was recorded at least 130 times in the 4 selected FI. Based on a synthesis of all our observations during dynamic and static measurements, we can say that nucleation at T_n is always marked by a rapid ‘jerk’ on the video image accompanied by a short perturbation of the temperature-recording device. Then, bubbles most generally coalesce in the narrowest part of the cavity. In negative crystal-shaped FI, bubble movement and coalescence is controlled by crystal edges. About 50 nucleation sequences were recorded with a high speed camera (200 images/s). The onset of nucleation was never observed even on recording at up to 900 images/s with a restricted field of view. When nucleation occurred at $T > T_n$, the nucleation process was all the shorter and the more limited in extent in the cavity volume as temperature was far from T_n .

II.7.2.b T_h and T_n reproducibility

Measurement reproducibility was as the whole good, within a few tenths of degrees. This is particularly true for the 4 selected FI, for which we have more than 30 T_h et T_n measurements. A shift in T_n was only recorded once in sample N31 FI 6. This sample was continuously maintained in the metastable liquid field for about one year, starting with experiment on FI 7 in February 2008 (El Mekki et al, 2010), and continuing by experiments on FI 6, then FI 26 and back to FI 7 from July to February 2009. T_n in FI 6 was measured at 52.1°C repetitively in winter 2006, winter 2007. During kinetic experiments on FI 7, FI 6 was superheated for 6 months 30°C above its T_n . In July 2008, its nucleation temperature had shifted by 4.7°C corresponding to a 3.7MPa decrease of its tensile limit. Its T_n subsequently remained unchanged (56.8°C).

II.7.2.c Explosivity

We here report about an unconventional kinetic experiment on metastable liquid water in a – 1 cm³ -sized N50 quartz fragment. which probably lead to the first explosive accident ever occurred with a microthermometric stage. The chosen prism volume was that required for a neutron diffraction study of tensile water in inclusions. A preliminary microthermometric study was necessary to measure the T_h 's and T_n 's of the FI, and to evaluate the range of tensile strengths of trapped liquid water and its lifetimes. In order to determine the latter parameters, the prism was directly placed on the silver block of the stage. A 200 µm- long and

20µm-wide FI exhibiting a Th at 298°C and Tn at 286°C (tensile strength ~ - 17 MPa) was placed at a tensile strength of MPa (Tstep= 288°C) and a first lifetime of about 16 hours was measured. The second kinetic measurement, required maintenance of the experiment overnight for lack of nucleation. The next morning, we found that the sample and the glass window were fragmented into pieces, the thermistance and the ceramics had molten, the temperature controller was damaged. Probably, the large volume of liquid water insufficiently confined into quartz was the cause of the explosive behaviour of metastable water in this sample. Also, it is possible that quartz has a lesser resistance to traction around large FI ~10⁴ µm³.

II.8 Kinetic results

II.8.1 Statistical treatment of lifetime series

Let T_{step} be the temperature above Tn at which an inclusion is stabilized in the metastable liquid state. Let t₀ be the time at which the temperature step begins (t₀ is taken as 0) and t_e > t₀ the time at which the vapour nucleation event occurs. Let t = t_e-t₀ be the metastable state lifetime. The variable t is continuous and characterized by a density probability function f(t) such that:

$$\int_0^{\infty} f(t) dt = 1 \quad (10)$$

According to the Classical Nucleation Theory, the repetitive formation of nuclei in a metastable liquid can be considered as a sequence of independent events and the distribution of lifetimes shows an exponential decrease (see also Takahashi *et al.*, 2002).

This implies that the density probability function f(t) of the nucleation event is:

$$f(t) = \lambda \times e^{-\lambda t} \quad (11)$$

where λ is the exponential decay constant.

If X is an exponential random variable, the probability that the vapour bubble nucleates within lifetime t is:

$$P(X \leq t) = \int_0^t \lambda e^{-\lambda x} dx = 1 - e^{-\lambda t} \quad (\text{Exponential Failure distribution}) \quad (12)$$

The probability of non nucleation of the vapour bubble within lifetime t is thus:

$$P(X > t) = e^{-\lambda t} \quad (\text{Exponential Reliability (or Survival) distribution}) \quad (13)$$

The exponential distribution has some major features. Like the radioactive decay rate, the nucleation rate is constant. The lifetime t does not depend on what happened before, i.e. the resistance to nucleation of a bubble at time t_0 does not depend on its resistance history before t_0 . The nucleation is a process “without memory”. This type of behaviour corresponds to the stationary hypothesis of the CNT. After reviewing some kinetic behaviours of inclusions, it was deduced that the exponential distribution of the metastability is not always verified. In one case, we observed an increase and in another a decrease of the lifetime along the successive experiments. For materials reliability, it corresponds to improvement or fatigue, i.e. the lifetime depends on history. The widely used Weibull distribution has a second parameter that measures this fatigue. The random variable X follows a Weibull distribution of second parameter β if X^β is exponentially distributed. $\beta < 1$ corresponds to improvement, $\beta > 1$ corresponds to fatigue.

We used SYSTAT 12 statistical software to check the exponential distribution of our experimental data. A series of tests were applied to all kinetic data sets of every studied FI. They were illustrated on Figure 6, with the statistical treatment of kinetic data at $t_{\text{step}}=152.2^\circ\text{C}$ of inclusion N16-FI 11

II.8.2 Statistical tests for stationary nucleation

The consistency of all lifetime data sets to an exponential decay law was verified on statistical grounds for the four selected FI. For example, kinetic data of inclusion N16-FI 11 best fitted the exponential decay law, as illustrated on Figure 6 for the 152.2°C T_{step} . Smoothing of the data (continuous curve, *Fig. 59a*) only showed random fluctuations and no increase or decrease of the duration of life with time. Also, these kinetic data near perfectly fit with the cumulative distribution function of an exponential law. The calculated p-value of the Kolmogorov-Smirnov test ~ 0.6 means that there are 60% chance to be wrong on stating that this data set is not stationary. The survival plots for two sub-series of the considered N16-FI 11 T_{step} appear visually coherent as their distributions functions overlap (*Fig. 59c*). The p-value of 9% and the value of 14%, show that the two subseries cannot be discriminated. Figures. 6d, 6e and 6f illustrate the results of the Monte Carlo simulations on the entire data set. The slight dissymmetry to the right of the distributions is characteristic of the Gamma law. In the case of inclusion N16-FI 1, the fit to a exponential distribution is perfect (*Fig. 59g*) whereas the fit to a Weibull distribution is of lesser quality (*Fig. 59h*) All lifetimes series

collected on our four FI have been shown to be consistent with an exponential decay law and stationary.

II.8.3 Mean lifetimes and nucleation rates.

Measured mean lifetimes of metastability (τ_{exp}) and calculated nucleation rates (J_{exp}) at each Tstep for every studied FI are reported in *Table 12*. Measured mean lifetimes in the selected FI are between - 50 and 63000s. Negative values were obtained, corresponding to relaxation of the tensile liquid occurring during the dynamic cooling part of the PT path (path 4 to 5, *Fig. 57*). These values were considered to be related to another physical process than the one studied at fixed Tstep>Tn, they were therefore rejected, as well as the zeros. In every FI, we tried to measure lifetimes of tensile water as close as possible to Tn. All our data however, were measured at 0.5°C from Tn or above (N31-FI 6 and N50-FI 1, *Table 12*). For instance, 50 % of measured lifetimes at Tn+ 0.5°C in FI 6 were negative. Closer to Tn, a majority of data were negative and had to be rejected. Occasionally, negative times were measured at Tn+1°C or Tn+2°C. Mean lifetimes in the studied FI ranged up to 24860 s (7 hours) at 7.5°C from Tn in N31-FI 6 to 63000s (~17 hours) at 6°C from Tn in N50-FI1. However, due to the high variability of measured lifetimes, some FI repetitively nucleated after one week or more at similar T-steps. The uncertainties shown in Figures are 50% confidence intervals.

Experimental data & interpretation								CNT model		
samples	Th (°C)	Tstep (°C)	Pstep (MPa)	ΔT	τ_{exp} (s)	γ (mN.m ⁻¹)	Jexp (m ⁻³ .s ⁻¹)	J(CNT) (m ⁻³ .s ⁻¹)	$\Delta F^*/k_B T$ CNT	r_c^* (CNT)
N31-FI 6	140.30	56.8	-114.66	0	-	78.31	-	1.81E-19	133.55	8.5E+35
	Ph	57.3	-114.19	0.5	192	78.16	9.01E+12	1.60E-19	133.67	9.6E+35
	0.36	58.3	-113.24	1.5	359	77.90	4.82E+12	9.39E-20	134.21	1.7E+36
	V(m3)	62.8	-108.87	6	7150	76.71	2.42E+11	7.67E-21	136.73	2.1E+37
	5.78E-16	64.3	-107.22	7.5	24860	76.22	6.96E+10	2.97E-21	137.68	5.4E+37
N31FI 26	Th									
	136.6	64.1	-102.41	0	-	76.82	-	1.26E-28	154.66	2.1E+43
	Ph(MPa)	65.1	-101.41	1	187	76.57	1.40E+13	4.51E-29	155.69	5.8E+43
	0.32	66.1	-100.32	2	208	76.31	1.26E+13	1.17E-29	157.04	2.2E+44
	V(m3)	67.6	-98.71	3.5	4000	75.73	6.54E+11	5.68E-30	157.77	4.6E+44
3.82E-16	69.1	-96.87	5	16700	75.24	1.57E+11	6.41E-31	159.95	4.1E+45	
N16-FI 11	Th									
	199.1	149.2	-78.07	0	-	57.34	-	1.33E+02	85.75	2.0E+12
	Ph(MPa)	151.2	-74.89	2	412	56.81	6.56E+11	1.85E+00	90.03	1.5E+14
	1.44	152.2	-73.3	3	2489	56.52	1.09E+11	1.97E-01	92.28	1.4E+15
	V(m3)	153.2	-71.71	4	14550	56.07	1.86E+10	4.31E-02	93.80	6.3E+15
3.7E-15	155.2	-68.53	6	63000	55.44	4.29E+09	3.45E-04	98.63	7.8E+17	
N50-FI 1	Th									
	283.7	262.2	-17.4	0	-	27.17	-	5.01E+05	77.75	2.2E+08
	Ph(MPa)	262.7	-16.8	0.5	26	27.01	4.27E+12	3.95E+04	80.29	2.8E+09
	6.782	263.2	-16.25	1	99	26.86	1.12E+12	3.72E+03	82.66	3.0E+10
	V(m3)	263.7	-15.7	1.5	2467	26.62	4.50E+10	6.43E+02	84.42	1.7E+11
9E-15	264.7	-14.6	2.5	37652	26.28	2.95E+09	3.38E+00	89.67	3.3E+13	

Tableau 12 : Experimental microthermometric measurements on the 4 inclusions, as a function of the “distance” to the T_n value. les données expérimentales : T_h , T_n , T_{step} , $T_{step}-T_n$, les durées de vie expérimentales (τ_{exp}) et on a déduit un taux de nucléation expérimentale J_{exp} avec l'équation 15. The water-vapor surface tension γ follows the “official” IAPWS equation. Les calculs CNT de facteur pré-exponentiel (J° et J°') calculé avec l'équation 6 et 7 respectivement, J selon l'équation 5 et ΔF à partir de l'équation 3. On a calculé ensuite des ΔF expérimentaux (ΔF_{exp}) et déduit les rayons critiques selon la loi de Young-Laplace. Calculations.

II.9 Interpretation and discussion

Variations of $\log(\tau)$ and $\log(J)$ as a function of ΔT i.e., ($T_{\text{step}}-T_n$) and ΔP , i.e., (P_n-P_{step}) are shown in figures 61 and 62, respectively. In an earlier paper, kinetic data for one FI were already plotted as a function of ΔT (El Mekki *et al.*, 2010). This is because T_n represents the tensile limit of every FI, it is the lower boundary of the metastability field for the considered trapped fluid. It separates static from dynamic metastability measurements. For each FI, measured $\log(\tau)$ and $\log(J)$ as a function of ΔT or ΔP plot along a straight line, a behaviour already observed over 6°C on a pure water FI (El Mekki *et al.*, 2010). The $\log(\tau)$ - ΔT plot (Fig. 61) only shows rough uninterpreted data. Also, since the τ 's are extensive variables, (they depend on the FI volume; e.g., Maris, (2006)), this plot describes each FI individually.. The data of every studied FI plot along a straight line. The plot appears fan-like, because the slope of the straight lines becomes all the steeper as the inclusion fluid is less tensile (N50-FI 1). This means that the lifetime of metastability increases as the fluid is less tensile. Also, the $\log(\tau)$ at T_n are all the smaller as the slope of the straight line is steeper (as the fluid becomes less tensile). The validity and significance of these measured τ at T_n , as well as the controlling parameters of metastability in individual FI, will be discussed in a second paper.

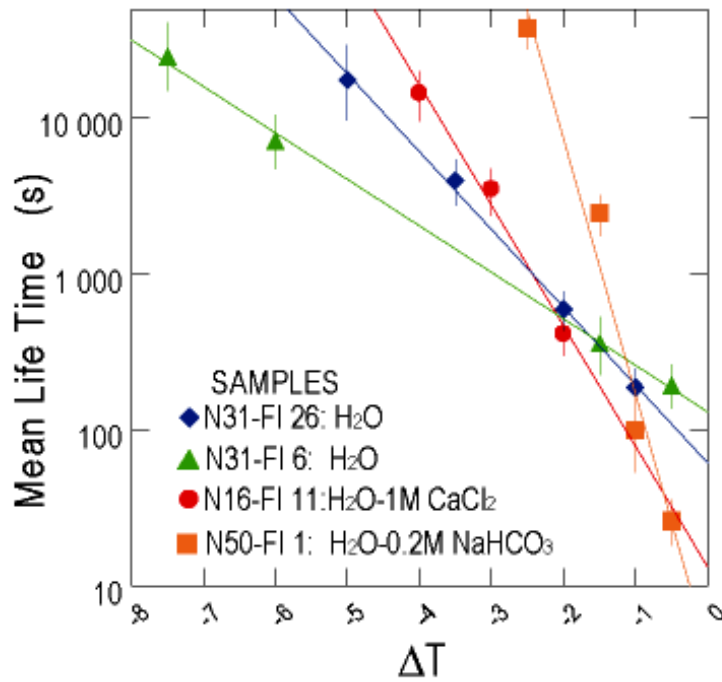


Figure 56 : (a) Lifetime with the decreasing liquid metastability ($\Delta T = T - T_n$). T_n corresponds to the maximum degree of metastability sustainable by the inclusions N31-6, N31-26, N16-11 and N50-1. (b) Evolution de Log (J) en fonction de ΔP des quatre inclusions.

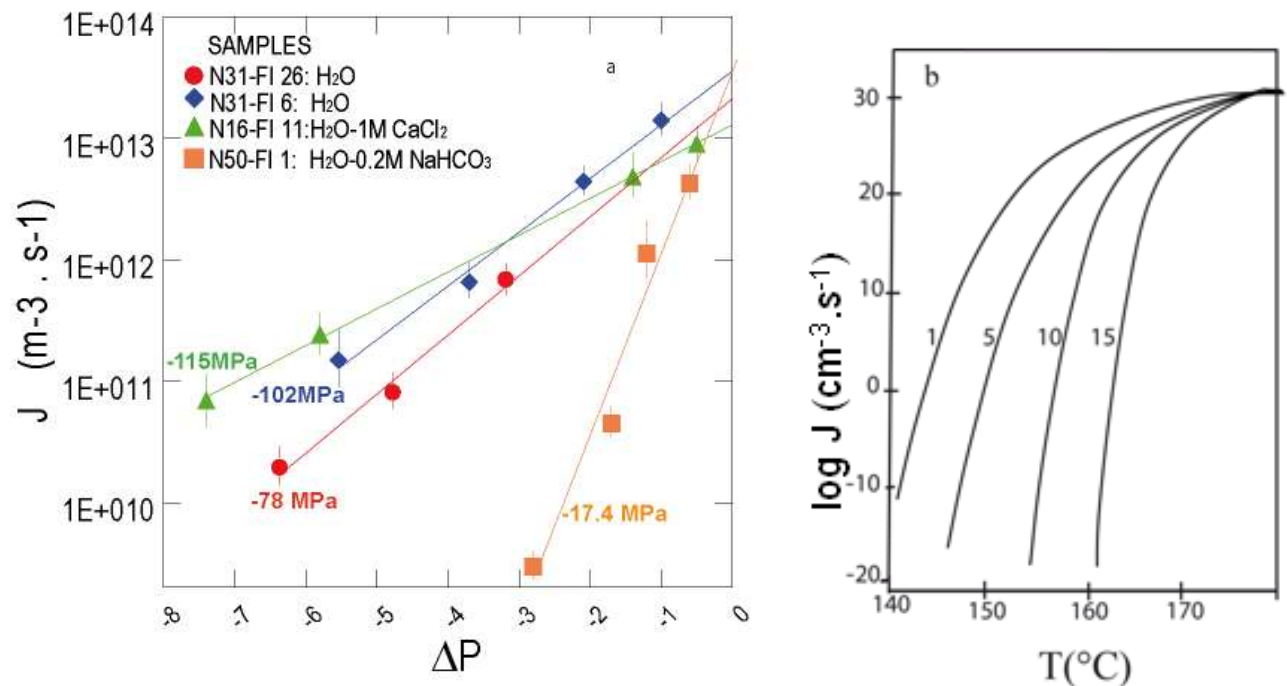


Figure 57 : (a) The nucleation frequency in superheated diethyl ether ($T_c = 193.5^\circ\text{C}$); (b) Calculations were according to Kagan's hydrodynamic theory. The labels on each curve were pressures in bar. (Debenedetti, 1996)

On Figure 8, calculated nucleation rates are plotted as a function of ΔP , the latter parameter being derived using the IAPWS-95 or the [Duan and Mao \(2006\)](#) EOS. Note that the J 's are specific variables, since the calculated rates are normalized per unit volume. The J 's illustrate the general behaviour of metastable trapped liquids in inclusions, independently of the size and shape of the cavities. The $\log(\tilde{J})-\Delta P$ projection more readily illustrates a specific feature of the limit of tensile water in FI : the convergence of the J 's towards a statistically defined unique value at T_n . This strongly suggests that the limit of tensile water in any FI occurs at a fixed nucleation rate $\sim 10^{13} \text{ m}^{-3} \cdot \text{s}^{-1}$.

The two FI which showed the most extreme tensile strengths in our selection (-115 for the pure water N31-FI 6 and -17.4 MPa for the NaHCO_3 -bearing N50- FI) yielded the flattest and the steepest line of the $\log(J)-\Delta P$ or $\log(J)-\Delta T$ plots, respectively (*Fig. 61*). These two FI have similar shapes, but they have very contrasted volumes and densities. N31-FI 7 ([El Mekki et al., 2010](#)) and N16-FI 11, which exhibit the same tensile strength, plot along same line on *Fig. 61*, despite the fact they have different chemistries (pure water and a 1M CaCl_2 solution, respectively), different densities and volumes (925 and 964 kg m^{-3} ; 8600 and $3700 \mu\text{m}^3$, respectively). These results suggest that the controlling parameter of the $\frac{\log J}{\Delta T}$ slope is the tensile strength of the liquid P_n and not density nor FI chemistry, even though the lines are isochoric not strictly isobaric. The slope K of the straight lines representative of every FI was linearly fitted as a function of P_n according to the equation $K = 4.37 - 0.03 \cdot P_n$. Note that previously published lifetimes on pure water FI 7, also originating from sample N31, fits with this equation. Thus, a generalized law for nucleation rates of tensile water in quartz-hosted FI can be proposed as follows:

$$\ln J = \ln [J(T_n)] + (4.37 - 0.03 \cdot P_n) \cdot (T - T_n) \quad \text{with } J(T_n) \sim 10^{13} \text{ s}^{-1} \text{ m}^{-3} \text{ and } \ln [J(T_n)] \sim 31$$

The only parameters controlling this kinetic law are, at least within 10MPa from P_n , the P , T and J at the tensile limit of the inclusion fluid: T_n , P_n , $J(T_n)$.

The inset in Figure 8a, reported by [Debenedetti \(1996, p. 183\)](#) after calculations by [Skripov \(1974\)](#), can be used as an aid to comment on the $\log(\tilde{J})-\Delta T$ plot. This inset shows nucleation rates of diethyl ether projected along isobaric lines as a function of T . The lines converge towards the critical temperature of diethyl ether, around 193.5°C , i.e., towards an invariant point of the phase diagram. This point is characterized by constant P and T , constant J , the vanishing of the liquid-vapour interface and of the related nucleation energy barrier. On *Fig. 61*, the J 's of metastable water in FI (i.e., along isochoric lines) converge towards a constant value of J , P and T at this saturation point are the P_n 's and T_n 's, all different for every FI. On

the other hand, this convergence point in FI corresponds to a metastability limit and not to an instability limit: an interface is present, corresponding to a non null energy barrier.

II.9.1 Comparison between measured mean lifetimes and CNT predictions.

Classical Nucleation Theory still remains a widely used reference model for metastable liquids (Xiao and Heyes, 2002; Oxtoby and Kashchiev, 1994; Debenedetti, 1996 ; Schmelzer, 2002 ; 2005 ; Maris, 2006 ;Herbert *et al.*, 2006; Vehkamäki, 2006). In *Table 12*, $\frac{\Delta F^*}{kT}$ were calculated at T_n and at the different T_{steps} for the 4 studied FI. Surface tensions were calculated using IAPWS-95 and taking in account the correction for interface curvature proposed by Melrose (1968). The J_{CNT} 's were then calculated using the exponential prefactor proposed by Turnbull (1949, 1950) and Fisher (1948) and hence the τ_{CNT} were deduced. *Table 12* shows that the mean lifetimes calculated with the CNT, comprised between 10^8 to 10^{45} s, are outside the range of experimental data. We can question why CNT fails to predict our kinetic data, whereas it was shown to correctly calculate the superheat limit of water at 302°C measured by Skripov (1974), and also the tensile strength of -140MPa reported by Zheng (1991) in one pure water FI at 45°C (Caupin and Herbert, 2006). This is because nucleation pressure is a less sensitive parameter than mean lifetimes for testing the CNT. Indeed, our experimental nucleation pressures are roughly to precisely calculated with CNT (taking in account the correction of curved interface; *Table 13* whereas the τ 's are widely overestimated. Surface tension is a critical parameter to account for liquid metastability (Balibar and Caupin, 2002). Besides, calculated J_{CNT} 's are very dependant on surface tension (see Davitt *et al.*, in prep.). We have therefore tested if CNT predictions and experimental data could be reconciled on varying the γ 's. The results were shown in *Table 13*. For N50-FI 1, with the lower tensile limit, CNT, predictions and experimental data are very close, there is nearly no need for adjusting the γ 's. By contrast, the higher the FI tensile limit is, the more the γ 's have be modified for the CNT predictions to fit with the data. *Table 13* presents the CNT model that has been successfully fitted on the experimental τ 's. This model can in turn be validated on another independent measured parameter, nucleation pressures, which it perfectly reproduces (*Tables 12* and *13*). Davitt *et al.* (in prep.), considering the CNT as a priori valid, then fitted the surface tension of tensile water so as to properly calculate an experimental P_n . In this

study, by combining independent dynamic and static measurements on tensile water, we could further validate the fitted CNT model on another experimental parameter.

Tableau 13 : Surface tension parameters γ adjusted on experimental mean lifetimes τ at T_n and every T_{step} for the four FI. The Table also shows recalculated $\Delta F^/kT$, J values and nucleation pressures P_{CNT}*

samples	τ (s)	recalculated γ (mN.m ⁻¹)	recalculated $\Delta F^*/kT$	recalculated $\Delta F^* E-19(J)$	J E13 (m ⁻³ .s ⁻¹)	P_{CNT} at T_n (MPa)
N31-FI 6	130	60,03	60,17	2,74	1	-119,6
τ at T_n (s)	192	60,02	60,57	2,76	0,9	
130	359	59,96	61,19	2,8	0,5	
	7150	59,62	64,19	2,98	0,02	
	24860	59,49	65,45	3,05	0,007	
N31-FI 26	36	55,55	58,48	2,72	7,45	-105,7
τ at T_n (s)	187	55,76	60,13	2,81	1,43	
61	208	55,45	60,24	2,82	1,28	
	4000	55,82	63,19	2,97	0,06	
	16700	55,63	64,66	3,05	0,01	
N16-FI 11	53	51,3	61,39	3,58	0,5	-82,0
τ at T_n (s)	412	50,5	63,43	3,71	0,06	
23	2489	50,37	65,23	3,83	0,01	
	14550	50,12	67,01	3,94	0,001	
	63000	49,09	68,48	4,05	0,0004	
N50-FI 1	4	24,9	59,87	4,42	3	-24,4
τ at T_n (s)	26	24,75	61,77	4,57	0,4	
4	99	24,55	63,14	4,67	0,1	
	2467	24,56	66,29	4,91	0,05	
	37652	24,1	69,08	5,13	0,0003	

We can confidently calculate the constant energy barrier $\frac{\Delta F^*}{kT} \sim 60$ for the formation of critical nuclei in tensile liquids trapped in FI. The fact this barrier significantly above zero confirms our previous statement that nucleation conditions in FI are not an instability limit ($\Delta F^* \neq 0$). Finally, we can conclude that, on simply changing the γ 's, our experimental linear fit of the J 's with T can be made compatible with the CNT model. This is not straightforward as the theoretical J 's are expressed as an exponential of a complex function of T . This point will be justified in part II paper.

II.10 Conclusions and geological implications

This paper has shown that, with a careful analytical procedure and an appropriate statistical methodology, microfluidic systems like fluid inclusions can easily provide good quality kinetic data on tensile water. Nucleation rates up to $2.4 \cdot 10^{21.5} \text{ m}^3\text{s}^{-1}$ were measured for metastable liquid water at positive pressure and a temperature of 302°C by the pulse heating method (Skripov, 1974). This paper reports measured nucleation rates of tensile water in synthetic FI of $\approx 10^{13} \text{ m}^3\text{s}^{-1}$. These values are inconsistent with the rates of $\approx 10^7 \text{ m}^3\text{s}^{-1}$ previously measured in the tensile domain by Takahashi et al. (2002) in 2 natural FI and they precise the value of $2.4 \cdot 10^{14} \text{ m}^3\text{s}^{-1}$ calculated with the CNT by Zheng (1991) in one FI at -140MPa and 45°C . With our set of data, we were able to validate the CNT model on simply changing surface tensions. This fact probably indirectly proves that measured nucleations in FI were homogeneous, since CNT strictly applies to homogenous nucleation. So far, the only objective criterion we had for homogenous nucleation was the fact that our T_n measurements were reproducible (Imre et al., 1998).

Our measurements demonstrate that nucleation rates at T_n are constant in any FI, whatever its volume, chemistry and fluid density, and at any $50^\circ < T_n < 280^\circ$ and $17 < P_n < 115 \text{ MPa}$. Thus, the fluid inclusion method to study metastability (a variant of the Berthelot's method) appears a constant flux method, in contrast to many others which are either high flux or low flux methods (Eberhardt, 1973; Eberhart et al., 1974; Debenedetti, 1996). From the constant value of J at $T_n \sim 10^{13} \text{ m}^3\text{s}^{-1}$, we have calculated, using our fitted CNT model, a constant energy barrier for tensile water in FI of $\frac{\Delta F^*}{KT}$ of ~ 60 , which seems to be valid over the whole negative P domain.

Can metastable water be invoked to interpret seismic data in the middle crust or can it influence fluid-rock interactions? We then have to question the extrapolation of our kinetic data, measured at up to 7°C of T_n and over time lengths of 10^5 s maximum, to temperatures up to 50° to 80°C from T_n along the isochore..and to time lengths of 10^9 s (i.e., a century : environmental conditions) and up 10^{13} s (1million years : geological conditions). Calculated nucleation rates of diethyl ester as a function of T using the CNT model below its critical temperature can be taken as an aid to answer this question. The diethyl ester model predicts exponentially-shaped isobaric lines over 40°C below the critical T (Fig. 6/b). It is possible that our linear $\log(J)$ versus T model becomes exponential over a larger T-range. Approximating an exponential curve by a line should yield overestimated values of J, and

hence minimized estimations of mean lifetimes. Thus we can deduce from our kinetic data that a fluid reservoir with a tensile limit of 100 MPa (Th below 200°C) can sustain , -85.5 MPa over one century minimum (corresponding $T = T_n + 15^\circ\text{C}$) and and -75 MPa over 1 million years minimum (corresponding $T = T_n + 22^\circ\text{C}$) respectively. This work therefore emphasizes that tensile water can be a major controlling-parameter of geochemical processes. Then, geochemists should consider attentively the numerous physical data on superheated liquid water at positive pressures, which have proven its highly changeable hydrophilic-hydrophobic properties (Lu *et al.*, 2002). Some Raman spectroscopic data have already confirmed a similar type of behaviour for water in the negative pressure field (Green *et al.*, 1990).

Acknowledgements — This work greatly benefited from the technical support of Laurent Perdereau who developed the hardware and software around the kinetic measurements. We are grateful to Frédéric Caupin (LPS, ENS Paris) and Yves Garrabos (Bordeaux) who continuously encouraged us and answered to our numerous questions. .This study received financial support from the French Agency for Research (Agence Nationale de la Recherche), grant SURCHAUF-JC05-48942 and from Russian Fund of Basic Investigations, grant 06-05-64460.

III kinetic stretched water and aqueous solutions in micrometric synthetic fluid inclusions:PART II: lifetimes and volumes

Mouna El MEKKI¹, Claire RAMBOZ¹, Jean-François LENAIN², Laurent Perdereau¹ and Kiril Shmulovich

¹Institut des Sciences de la Terre d'Orléans, UMR 6113 CNRS/Universités d'Orléans et Tours, 1A rue de la Férollerie, 45071 Orléans Cedex

²Université de Limoges, Groupe de Recherches Eau Sol Environnement (GRESE), 123 avenue Albert Thomas 87060 Limoges, France.

³Institute of Experimental Mineralogy, Russian Academy of Science, 142432 Chernogolovka, Russia.

* Corresponding author: Mouna.Elmekki@cnrs-orleans.fr

III.1 Introduction

Fluid inclusions (FI) are very convenient microfluidic systems to study confined metastable water and solutions, based on the same principle as the Berthelot vase (1850). Recently, a large set of FI displaying a wide range of densities (965 to 825 g.m⁻³), containing pure water and moderately to highly saline salt solutions, with various cations from Na, Ca and Cs, were

synthetized specifically for the latter purpose. A first paper explored the tensile limits of water in these FI and determined extreme nucleation pressures (P_{cav}), sometimes still to be quantified in the case of CsCl-bearing FI (Shmulovich et al., 2009). El Mekki et al. (2010; submitted), subsequently continued this exploration of the tensile domain of water and solutions on measuring lifetimes of water under negative pressure in 5 selected FI. They were able to propose an empirical equation for calculating nucleation rates J in FI within a pressure range of 10 MPa above P_{cav} in the range 17-115 Mpa. The papers by Shmulovich et al. (2009) and El Mekki et al. (2010; submitted) have exploited two advantages of the FI method: the capability to allow both dynamic and static measurements, i.e., measurements at controlled cooling rates and at constant temperatures, respectively. In this regard, it is worth noting that dynamic and static experiments have given access to different kinds of parameters so far : nucleation temperatures (T_n) and pressures (P_n or P_{cav}) on the one hand, lifetimes τ on the other hand. T_n , P_n and τ are size-dependant since the probability of nucleation depends on the FI size (e.g., Maris et al. 2006). In a previous paper, we considered J 's, which are specific quantities, normalized per unit volume. In this paper, we want to consider the metastable behaviour of each FI individually, and analyze in more detail the controlling parameters of metastability in each of them. We shall also justify the constant nucleation rates at T_n that were obtained on extrapolating kinetic data to the tensile limit T_n for every FI.

III.2 Methods of estimations of fluid inclusion volumes

The methods for measuring the FI volumes and the results obtained have been presented in Chapter IV (in French). They will be translated and integrated later in this paper.

III.3 Results

We summarize the main relationships observed between FI volumes and their tensile limits. Negative crystal shaped inclusions will not be considered below, because their specific behaviour is beyond the scope of this paper. On Figure 63, the expected behaviour of increasing tensile limits of water as the FI volume increases is shown. However, rounded, tubular and more complex-shaped FI plot along different lines of the $\log V - T_n - T_h$ plot, depending on their shapes.

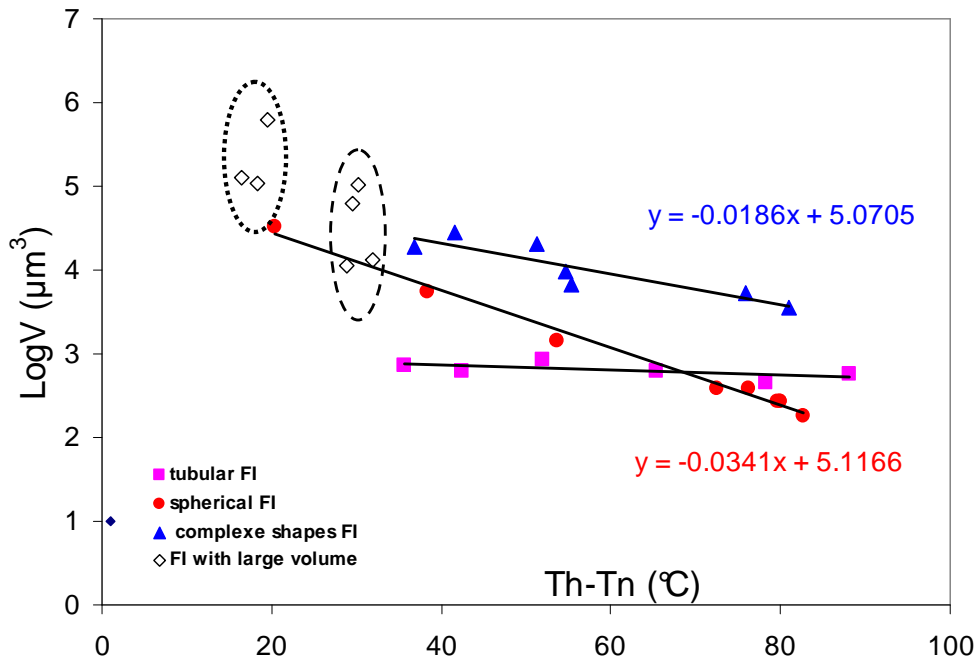


Figure 58 : Sample N31 pure water fluid inclusions. (a) LogV versus (Th-Tn) plot. Red dots : rounded FI. Blue triangles: complex shaped FI with one dimension $\geq 10 \mu\text{m}$. Pink squares: tubular FI with fixed widths of $5 \pm 1 \mu\text{m}$. For the rounded and tubular FI, the diameters and calculated values of $\tau(T_n)$ are indicated for the smaller and larger FI and in s, respectively (in μm and s, respectively)

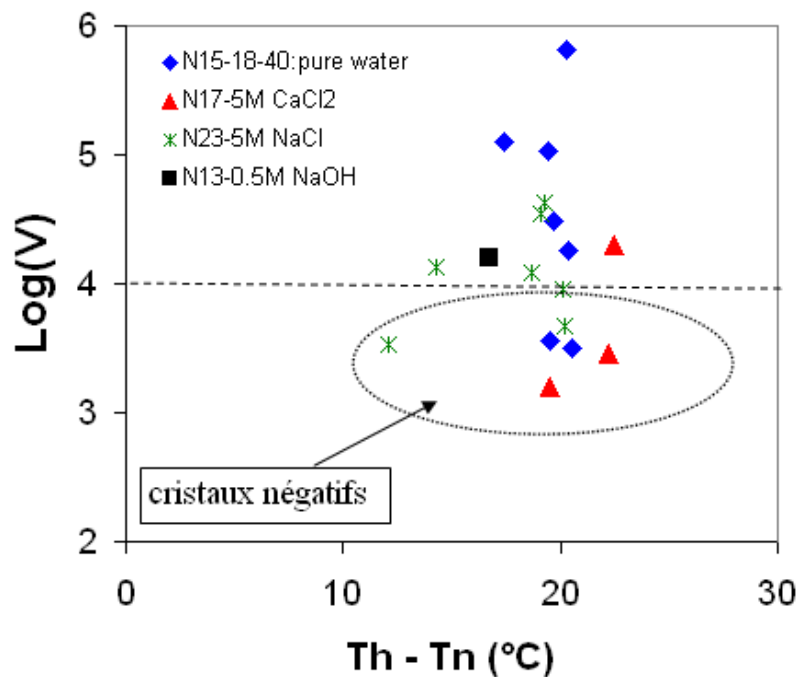


Figure 59 : LogV versus (Th-Tn) plot of FI with $(Th-Tn) \sim 20^\circ\text{C}$, corresponding to low tensile strengths $\sim -35 \text{ Mpa}$. These FI are characterized by volumes $\geq 10,000 \mu\text{m}^3$.

On the other hand, for the FI the volume of which is larger than $\sim 10,000 \mu\text{m}^3$, the tensile limit remains low ($\sim -35 \text{ MPa}$) and independent of the FI volume Fig. 64).

III.4 Discussion

III.4.1 Calculation of $\tau(T_n)$ from rate-controlled T_n - V measurements.

The formalism used here was established by Skripov (1974) to interpret rate-controlled heating experiments on water droplets in the positive pressure domain, and developed by Blander and Katz (1974); Eberhart et al. (1975); Debenetti (1996).

Let N_0 be the density number of water, let N be the number of critical nuclei in a given volume V . Let the experiment occur at a controlled rate $\frac{dT}{dt}$. The decay rate of critical nuclei during a time interval dt can be expressed as follows, according to the Survival law (or the Boltzmann equation):

$$dN = -N_0 J V dt \quad (1)$$

where J is the nucleation rate.

Introducing the constant heating rate $\frac{dT}{dt}$, it follows:

$$\frac{dN}{N_0} = \frac{-JV}{\left(\frac{dT}{dt}\right)} dt \quad (2)$$

Let us integrate relation (2) along a cooling path from room temperature (where the probability of nucleation is 0) to T_n (we consider that the fluid cavitates when $\frac{N}{N_0} \approx 0.5$). We

have:

$$\text{Ln}(0.5) = \frac{-V}{\left(\frac{dT}{dt}\right)} \int_0^{T_n} J dT \quad (3)$$

El Mekki et al. (submitted) have established that within 10 MPa of T_n , J could be approximated by the relation: $\text{Ln}(J) \sim \text{Ln}[J(T_n)] - LT$. This approximation was also proposed by Skripov (1974). Hence

$J \sim J(T_n) \exp(-LT)$. It follows :

$$\text{Ln}(0.5) = \frac{-V \times J(T_n)}{L \left(\frac{dT}{dt} \right)} \quad (4)$$

El Mekki et al. (submitted) determined from their kinetic experiments that $J(T_n)$ in FI was a constant s equal to $10^{13} \text{m}^{-3} \cdot \text{s}^{-1}$. Hence L , the temperature dependence parameter, can be calculated as a function of the FI volume V and as a function of the cooling rate of the experiments (equation (4)) as follows:

$$L = \frac{V \times J(T_n) \times \text{Ln}2}{\left(\frac{dT}{dt} \right)} \quad (5)$$

Let $\tau(T_n)$ be the median lifetime of tensile water at T_n . We have:

$$\tau(T_n) = \frac{\text{Ln}2}{V \times J(T_n)}. \quad (6)$$

The temperature dependence parameter L calculated after equation (5) is shown in Table 1, together with the experimental L -values taken as the slopes of the straight lines $\text{Ln}(J)$ versus $(T-T_n)$ for the 4 FI (not shown). Median lifetimes $\tau(T_n)$ calculated after equation (6) are also shown together with the experimental $\tau(T_n)$ -values (taken as the intercepts at $T = T_n$ of the straight lines $\text{Ln}(\tau)$ versus $(T-T_n)$). The consistency between measured and calculated $\tau(T_n)$ is quite good whereas the agreement between calculated and measured L is lesser.

The accuracy on the $\tau(T_n)$'s probably relies on two factors: (1) The calculation of $\tau(T_n)$ involves $J(T_n)$ and this parameter has been well constrained by careful static measurements (El Mekki et al., submitted). (2) A precise knowledge of T_n is essential for the treatment of kinetic data as this temperature is the boundary of the metastability field for the considered FI. The consistency between the two sets of $\tau(T_n)$ is an indirect indication of the proper evaluation of T_n , the tensile limit of the FI. The calculation of L by contrast depends on the cooling rate. Probably the estimation of the static parameter L referring to a parameter from

the dynamic part of the path $\left(\frac{dT}{dt} \right)$ introduces a large uncertainty.

Tableau 14 : Calculation of the temperature dependence parameter L , and of normalized L per unit volume, where V is the FI volume.

Inclusion number	FI volume (m ³) X10 ¹⁶	Cooling Rate (°C.s ⁻¹)	L (K ⁻¹)	$L/V \times 10^{-15}$ (K ⁻¹ m ⁻³)	calculated $\tau(Tn)$ (s)	measured $\tau(Tn)$ [°] (s)
N31-FI6	5.78	0.03	0.28	0.48	120	130
N31-FI26	3.82	0.03	0.18	0.48	181	61
N16-FI11	37	0.03	1.80	0.48	19	23
N50-FI1	90	0.08	1.63	0.18	8	4
N50-FI1	90	0.03*	4.35*	0.48*	8	4

°: after El Mekki et al. (submitted); *: recalculated for a cooling rate of 0.03 °C/s

III.4.2 Parameters controlling the tensile limit of inclusion fluids.

A previous paper on the kinetic behaviour of tensile water in FI has shown that the main controlling parameter of lifetimes of metastability is the tensile limit of the inclusion fluid. A major point to consider therefore is what fixes the Pn , Tn , $\tau(Tn)$ characteristic features of FI.

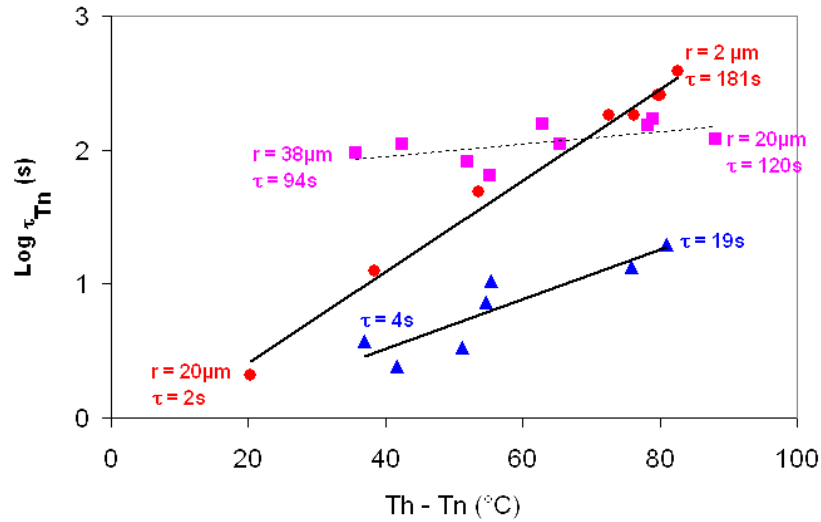


Figure 60 : Sample N31 pure water fluid inclusions. $\text{Log } \tau(T_n)$ versus $(Th-T_n)$ plot. Symbols as in Fig.1. For the rounded and tubular FI, the diameters and calculated values of $\tau(T_n)$ are indicated for the smaller and larger FI, in μm and s, respectively.

Figure 65 allows to visualize how vary the sizes and shapes of FI as they plot deeper in the tensile field along a single isochore. Tubular, rounded and more complex-shaped FI define linear trends in the $\text{log}V - (Th-T_n)$ diagram, however all of them whatever their shape, define a similar range of tensile limits between 37 and 115 MPa. The volumes of tubular FI vary in a small interval compare rounded FI, the volumes of which vary over 3-4 orders of magnitude (in log). This is normal as the plotted tubular FI have a constant section and variable lengths, whereas the volume of the rounded FI varies as a function of r^3 . The two lines of rounded and tubular FI intersect at a point where a tube and a spherical FI have the same $V \sim 900 \mu\text{m}^3$, and show a similar range of metastability $(Th-T_n) \sim 70^\circ\text{C}$. At lower $(Th-T_n)$, for a given tensile strength, the spherical shape will host a larger volume of metastable fluid than the tube. Beyond the intersection point $(Th-T_n)$, the tubular FI will host a larger fluid volume than the sphere. Let us introduce a dimensionless ratio S^3/V^2 to further characterize the inclusion forms (S and V are the surface area and volume of the shape, respectively). Figure 2 shows that sphere is a shape characterized by constant S^3/V^2 . It is also the shape that has encloses the largest volume in the smallest surface. The line defined by the rounded FI in the $\text{log}V - (Th-T_n)$ diagram (Fig. 66) is a constant S^3/V^2 line, where one can visualize the effect of the volume decrease at constant S^3/V^2 on increasing the tensile strength of the inclusion. A

decrease in the FI volume by $1400\mu\text{m}^3$ will result in an increase of the tensile strength of ~ 14 MPa

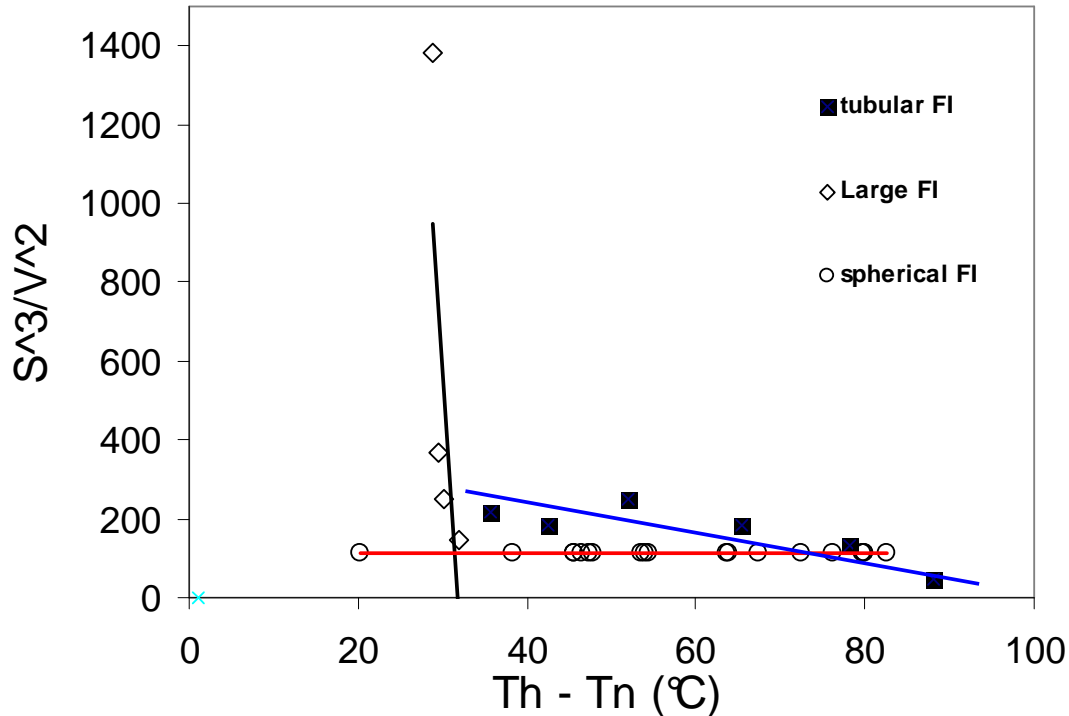


Figure 61 : Dimensionless ratio S^3/R^2 of the spherical and tubular aqueous FI as a function of $Th-Tn$ ($^{\circ}\text{C}$). S = surface area of the FI; V : cavity volume. Also shown are some representative points of large tubular FI synthesized at 365°C and 160 MPa in $\text{H}_2\text{O}-0.5\text{M NaOH}$ solutions.

The S^3/V^2 parameter in tubular FI decreases as $(Th-Tn)$ increases. On figure 2, the line of rounded FI intersects the line of tubular FI at $(Th-Tn) \sim 70^{\circ}\text{C}$. Hence we conclude that, at constant tensile strength, the FI shape that has the lowest S^3/V^2 parameter will contain the larger volume of metastable fluid. Similarly, at constant volume, it will show a larger tensile limit. The tubular FI are a case where a small volume decrease of $45\mu\text{m}^3$ induces a spectacular decrease of 140 MPa of the tensile strength. However, its S^3/V^2 simultaneously decreases from 200 to 170 : this proves that decreasing the S^3/V^2 of an inclusion shape strongly increases the tensile strength of the fluid it hosts. Judging from their characteristic slope in the $\log V - (Th-Tn)$ plot, nearly parallel to that of rounded FI, the complex-shaped FI should display near constant S^3/V^2 . Finally, the largest FI, the tensile strength of which is fixed at $\sim 35\text{ MPa}$ independently of the FI volume $> 10000\mu\text{m}^3$, show vertically increasing

S^3/V^2 values. Figures 1 and 2 thus show that when the shape of a FI is dominated by its surface area relative to its volume, the fluid it hosts will display a low tensile strength.

In Figure 65, the $\log V - (T_h - T_n)$ plot has been converted to a $\log(\tau(T_n)) - (T_h - T_n)$ diagram, according to equation (6). Figure 6 illustrates the fact that $\tau(T_n)$ is a parameter inversely proportional to volume. In the largest FI, $\tau(T_n)$ are close to 0 whereas the tubes with a fixed section of 5 μm in diameter, display $\tau(T_n) > 90$, even in the low tensile range, where $\tau(T_n)$ in rounded FI is near 0.

III.5 CONCLUSIONS

In this paper, we have paid attention to the consistency between measurements on metastable water in FI at controlled cooling paths (P_n , T_n , $\tau(T_n)$) and the lifetimes measured under static conditions. We found a good consistency between the Skripov's approach of the dynamic part of metastability studies (1974) and extrapolated parameters to T_n deduced from kinetic measurements at $T > T_n$. A major point for understanding the behaviour of tensile water in fluid inclusions is to understand the controlling parameters of the tensile limit of trapped water. We have shown that the volume and the shape of FI controls their tensile limits. A major stereologic parameter of FI shape is the dimensionless ratio S^3/V^2 . At near constant volume, increasing this ratio by 15% in tubes induces a decrease in the tensile limit of the hosted fluid by around 21%. By contrast, a much larger increase in the volume of a FI is required to induce a similar decrease in the fluid tensile limit. Shapes which enclose the largest volume in the smallest surfaces, like spheres, are favourable to increased tensile limits of the hosted fluid. By contrast, shapes the surface of which increases more rapidly than volume, are not favourable hosts for highly tensile liquids. The parameter $\tau(T_n)$, also characteristic of individual inclusions, is inversely proportional to FI volume. It amounts to a few hundreds seconds in 300 μm^3 - sized FI. We suggest that high $-\tau(T_n)$ values could be indicative of capillary forces in FI. This parameter can be calculated precisely in individual FI taking in account the constant nucleation rate at T_n of $10^{13} \text{ m}^{-3} \cdot \text{s}^{-1}$ kinetic measurement (El Mekki et al., submitted). We showed that the use of mathematical morphology computer programs can help predicting the tensile limit of water in individual FI. Some negative crystal

shaped FI may host large volume of fluids with high tensile limits. The tensile strength of water may increase as the FI volume increases. Metastable water in these faceted FI with edges requires a specific study.

IV Mesure cinétique dans une inclusion de dislocation

Pour confirmer les résultats obtenus par les mesures de cinétique, on a voulu vérifier le comportement cinétique des IF qui se trouvent dans le domaine métastable restreint, limité par le domaine critique et la courbe spinodale. Pour réaliser cette étude, on a choisi une IF à faible P_n , synthétisée avec une technique différente que celle de Kiril Shmulovich. Le but de ce choix étant de vérifier l'influence de la technique de synthèse sur la gamme de métastabilité et sur la durée de vie des IF métastables.

IV.1 Cristal utilisé et technique de synthèse

Les IF se trouvent dans un quartz synthétique. Ce quartz a été échantillonné à la SICN (Annecy, France). Les analyses de spectrométrie IR ont montré que ce minéral contient probablement moins de 300 ppm d'OH dissous dans le réseau, ce qui est responsable de son dessèchement.

Ce quartz a été synthétisé par croissance hydrothermale à $T = 365^\circ\text{C}$ et à $P = 160\text{MPa}$, dans une solution de 0.5M $\text{H}_2\text{O-NaOH}$, autour d'un germe allongé selon un axe a et aplati perpendiculairement à l'axe c . Les IF obtenues sont de forme cylindrique, de grande taille et allongées suivant une direction proche de l'axe c . Les analyses par tomographe ont montré que ces IF se sont formées par corrosion du cœur des longues dislocations très rectilignes contenues dans le germe, avant que la saturation ne soit atteinte dans l'autoclave grâce à un mécanisme évoqué par [Wilkins et McLaren \(1981\)](#). La croissance de quartz et le piégeage des IF ne se réalisent qu'après que la saturation atteint les conditions de synthèse dans l'autoclave. Le fluide ainsi piégé égale à la densité du fluide dans l'autoclave ([Pécher et Boullier, 1984](#)).

IV.2 Microthermométrie

L'échantillon contenant la section de germe a été coupé à l'aide d'une micro-scie et poli pour éviter les irrégularités de la surface. Le fragment de quartz obtenu a une épaisseur moyenne d'environ $500\mu\text{m}$ et contient des IF tubulaires et grande taille. Les volumes de IF sont importants et variables entre 1.1×10^{-14} et $1.06 \times 10^{-13} \text{ m}^3$. Ce fragment a été placé dans la

platine THMS 600 et les T_h et T_n ont été mesurées suivant le même protocole utilisé dans ce travail. Les T_h ainsi obtenues sont variables entre 242° et 243°C , très proche de la valeur de 245°C obtenue par Pécher et Boullier (1984) dans le même type d'échantillon. Les T_n trouvées sur les IF sont variables entre 211° et 214.5°C et les gammes de métastabilité sont comprises entre 29.6° et 32°C . Les P_n ont été calculées à partir de l'EOS de l'eau pure (Wagner et Pruss, 2002) car la solution aqueuse occlus dans les IF est faiblement concentré. Les P_n ainsi calculées sont comprises entre -31 et -35MPa . On a réalisé des mesures microthermométriques extensives sur une IF de dislocation (Fig. 67).

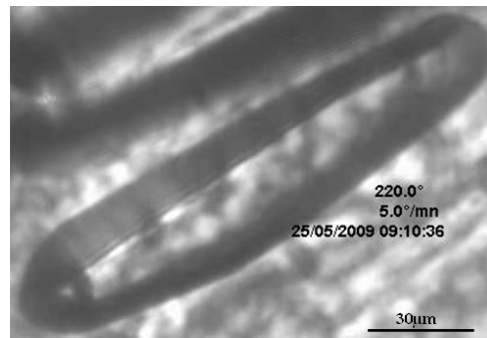


Figure 62: Photo de l'IF à 0.5M H₂O-NaOH, synthétisée par corrosion du cœur de dislocation, pendant le chauffage (x32).

Les T_h et T_n sont reproductibles et égales à 242.4° et 212.2°C respectivement. La P_n calculée pour cette IF est de -37.4 MPa . Cette IF a servi pour réaliser l'étude de cinétique et les temps de vie ont été mesurés à quatre paliers de température à : 1° , 1.5° , 2° et 2.5°C de la T_n .

IV.3 Résultats et conclusions

Les résultats obtenus (Fig. 68 et 69) sont en parfait accord avec les résultats acquis précédemment. Cette IF de faible degré de surchauffe a pratiquement le même comportement que la N50-IF1 (à -17.4MPa). La cinétique de l'IF de dislocation montre aussi une convergence vers la valeur de $J = 10^{13}\text{ m}^{-3}\cdot\text{s}^{-1}$ à la T_n . Ceci confirme que la durée de vie dans les IF ne dépend que son degré de métastabilité. Pour cette IF, on a validé la CNT et la P_n de -37.5 MPa calculée par l'EOS.

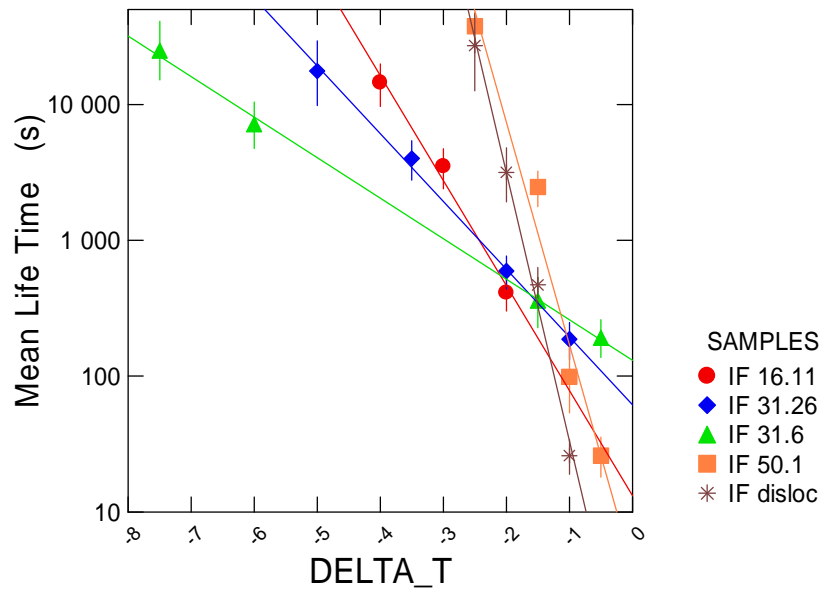


Figure 63: Temps de vie dans les inclusions fluides métastables en fonction de l'éloignement par rapport à T_n .

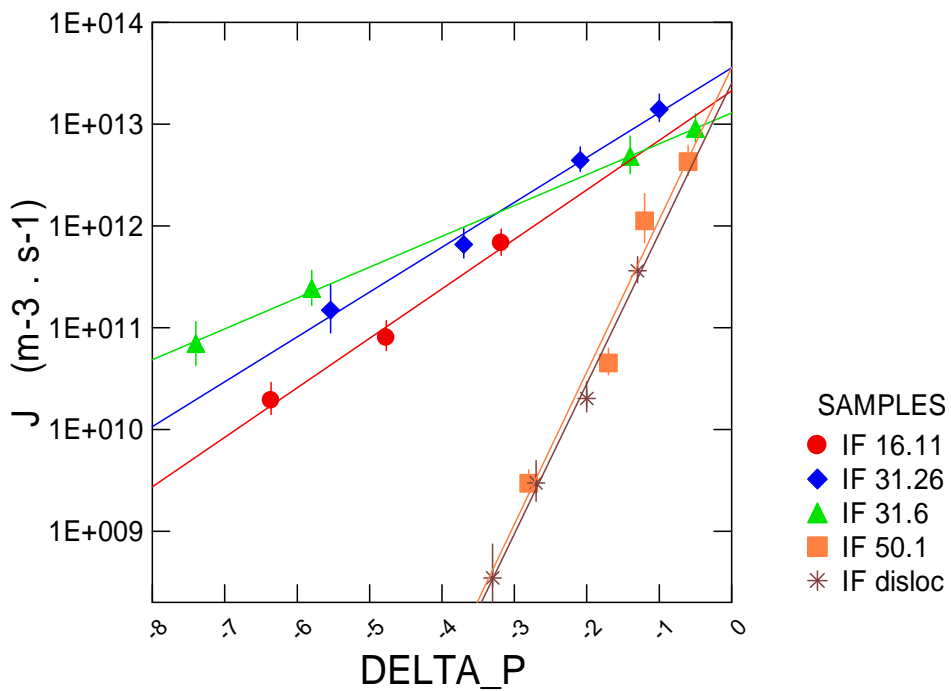


Figure 64: Taux de nucléation calculés pour chaque palier de température en fonction de l'éloignement par rapport à la pression de nucléation.

Les gammes de surchauffe obtenues dans les IF de dislocation sont plus importantes que celles obtenues dans les IF de même volume, synthétisées par Kiril Shmulovich. Le N50-IF1 de même forme et de volume plus petit a une Pn plus petite que l'IF de dislocation étudiée. Très probablement, le mode de synthèse par puits de dislocation efface les défauts de surface et freine la nucléation dans les IF. Le changement de la technique de synthèse et de la solution de fluide occlus n'a aucun effet sur la durée de vie ; seul le degré de métastabilité compte, plus celui-ci est petit plus la durée de vie de l'état tensile dans l'IF est longue et vice versa. *Cette étude fait l'objet d'un article (part III) en cours de préparation.*

V Cas particulier de la cinétique dans les inclusions fluides synthétiques

Grace aux mesures de cinétique sans interruption et aux traitements statistiques, on a observé deux cas particuliers dans les IF où le temps de vie change aux cours de temps (de l'expérience). Le 1^{er} cas a été suspecté sur le necking down N31-IF7 (El Mekki *et al.*, 2010). Dans la première étude, le nombre limité des mesures réalisées d'une façon discontinue (arrêt pendant les nuits et les week end) sur cette IF n'ont pas permis de remarquer un changement de τ au cours de temps, mais, certaines grandes valeurs en fin de mesure ont été suspectées. Après avoir intégrer les règles statistiques et changer le protocole expérimentale (mesures sans interruptions), on a repris les mesures sur la N31-IF 7. Le 1^{er} test de la moyenne glissante obtenu dans la figure 70 (comparé à un cas exponentiel normal dans la figure 70a) montre l'augmentation des τ aux cours de temps. Ce test visuel est suffisant pour montrer le non conformité à la loi de fiabilité. L'IF 7 a un comportement de bonification qui suit la loi Weibull (Fig. 70b). En revanche, le cristal négatif N32-IF 7 à H₂O-0.1M NaOH, lui suit une loi weibull qui montre une fatigue aux cours de temps (Fig. 70c). *Un article en préparation est dédié à ces cas particuliers en cinétique tout en insistant sur l'importance de la méthode expérimentale imposée par les règles statistiques.*

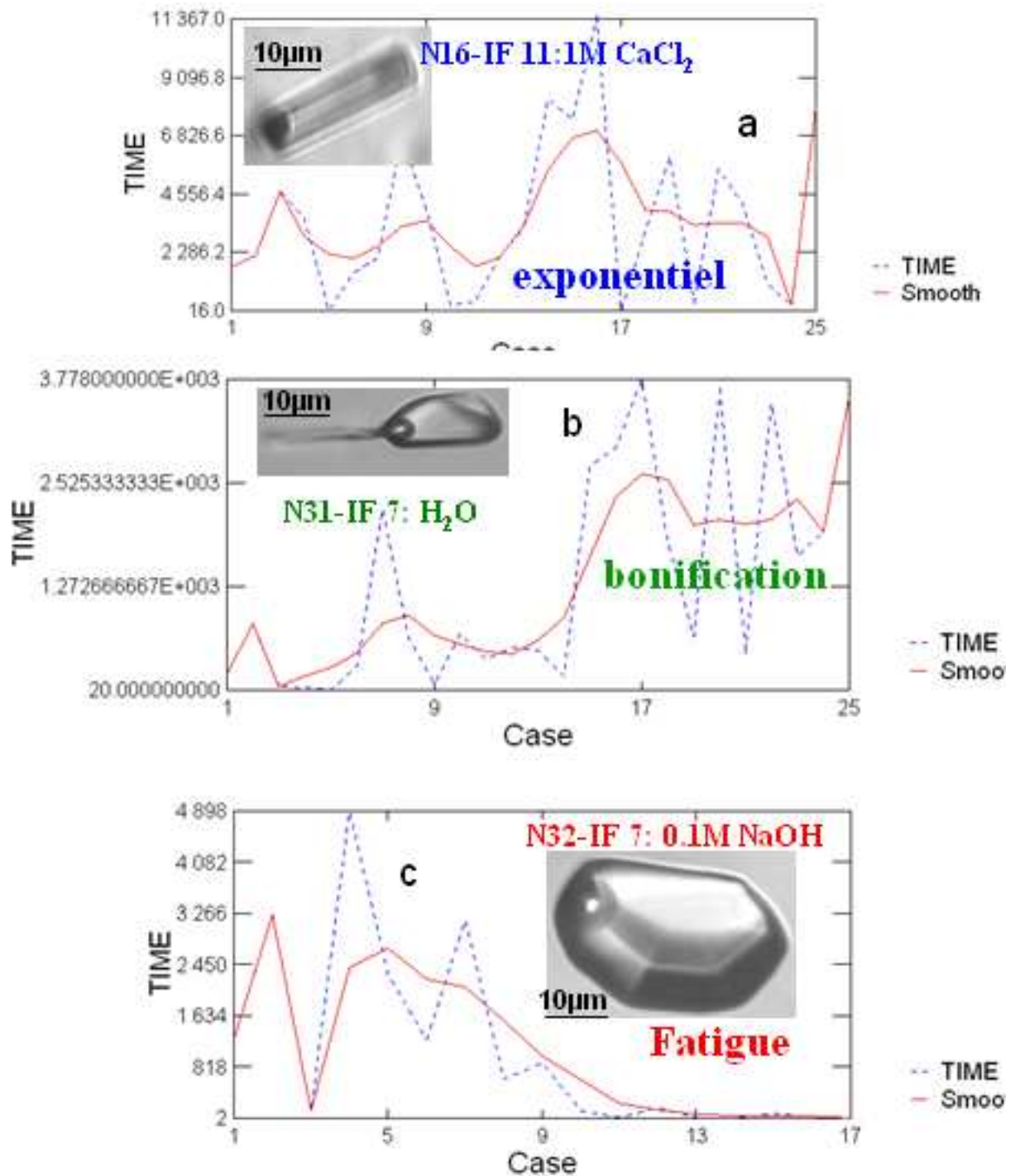


Figure 65 : Le test de la moyenne glissante réalisé sur 25 mesures pour un pallier de température donné ; (a) une moyenne glissante normale (exponentielle) sur N16-IF 11 servant de témoin de la conformité à la loi de survie ; (b) une bonification dans le necking down N31-IF 7 et (c) une fatigue dans le cristal négatif N32-IF 7 aux cours de temps.

VI Cas particulier de la cinétique dans une IF naturelle de l'anhydrite de la Mer Rouge

Une série de mesures microthermométriques a été réalisée sur des inclusions fluides naturelles à 17.8% NaCl. Ces dernières sont piégées dans un cristal d'anhydrite provenant de la Mer Rouge Centrale (Fig. 71) Ces mesures ont été difficiles à cause d'un phénomène de décrépitation très fréquent. Pour éviter ce problème, on a limité les mesures de Th et Tn sur 14 IF ayant un taux de remplissage n'excédant pas ~10%. Les Th et Tn ont été très peu variables et de l'ordre de 107.2° et 66°C, respectivement.

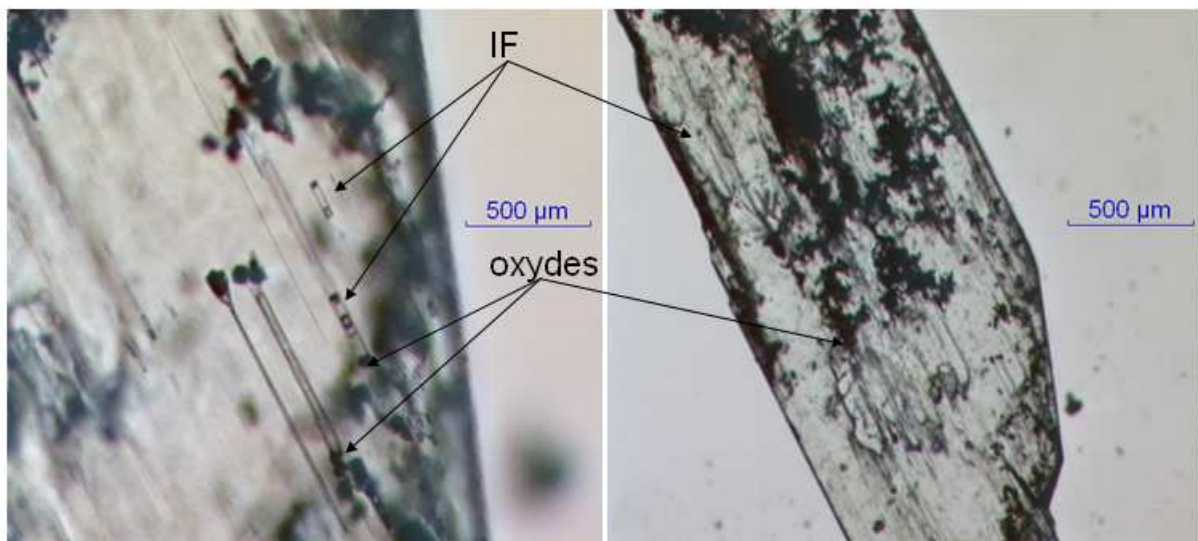


Figure 66 : Inclusions fluides dans un cristal d'anhydrite (A16) provenant de la Mer Rouge.

On a réalisé des mesures de cinétique sur une seule IF de densité initiale de 1040 kg.m^{-3} et un volume de $\sim 1562 \text{ }\mu\text{m}^3$. Pendant un mois de mesure, cette IF a changé 5 fois de Th et Tn (elles sont devenues plus importantes), et un très grand nombre de mesures non exploitables de τ ont été obtenues. La mesure de la métastabilité à pression négative n'est pas concluante dans les IF piégées dans des cristaux clivables, car des microfissures se forment facilement et les cristaux ne sont plus étanches.

*Implications de la métastabilité pour le
milieu naturel*

